Monthly Notices of the ROYAL ASTRONOMICAL SOCIETY

MNRAS **536,** 3159–3176 (2025) https://doi.org/10.1093/mnras/stae2716
Advance Access publication 2024 December 16

The High Time Resolution Universe Pulsar Survey – XIX. A coherent GPU-accelerated reprocessing and the discovery of 71 pulsars in the Southern Galactic plane

R. Sengar,[1,2,3,4,5★] M. Bailes,[1,2] V. Balakrishnan,[6] E. D. Barr,[6] N. D. R. Bhat,[7] M. Burgay,[8] M. C. I Bernadich,[6] A. D. Cameron,[1,2] D. J. Champion,[6] W. Chen,[6] C. M. L. Flynn,[1,2] A. Jameson,[1,2] S. Johnston,[9] M. J. Keith,[10] M. Kramer,[6,10] V. Morello,[10] C. Ng,[11] A. Possenti,[8,12] S. Stevenson,[1,2] R. M. Shannon,[1,2] W. van Straten[13] and J. Wongphechauxsorn[6]

[1]*Centre for Astrophysics and Supercomputing, Swinburne University of Technology, Mail H39, PO Box 218, Hawthorn, VIC 3122, Australia*
[2]*ARC Centre of Excellence for Gravitational Wave Discovery (OzGrav), Swinburne University of Technology, Mail H11, PO Box 218, Hawthorn,VIC 3122, Australia*
[3]*Center for Gravitation, Cosmology, and Astrophysics, Department of Physics, University of Wisconsin-Milwaukee, PO Box 413, Milwaukee, WI 53201, USA*
[4]*Max Planck Institute for Gravitational Physics (Albert Einstein Institute), D-30167 Hannover, Germany*
[5]*Leibniz Universität Hannover, D-30167 Hannover, Germany*
[6]*Max-Planck Institut für Radioastronomie, Auf dem Hügel 69, D-53121 Bonn, Germany*
[7]*International Centre for Radio Astronomy Research, Curtin University, Bentley, WA 6102, Australia*
[8]*INAF - Osservatorio Astronomico di Cagliari, Via della Scienza 5, I-09047 Selargius (CA), Italy*
[9]*CSIRO Astronomy and Space Science, Australia Telescope National Facility, PO Box 76, Epping, NSW 1710, Australia*
[10]*Jodrell Bank Center for Astrophysics, University of Manchester, Alan Turing Building, Oxford Road, Manchester M13 9PL, UK*
[11]*Dunlap Institute for Astronomy and Astrophysics, University of Toronto, 50 St George Street, Toronto, ON M5S 3H4, Canada*
[12]*Department of Physics, Università di Cagliari, SP Monserrato-Sestu Km 0,700, 09042 Monserrato, Italy*
[13]*Institute for Radio Astronomy and Space Research, Auckland University of Technology, Private Bag 92006, Auckland 1142, New Zealand*

Accepted 2024 November 28. Received 2024 November 28; in original form 2024 June 11

ABSTRACT

We conducted a GPU-accelerated reprocessing of ~ 87 per cent of the archival data from the High Time Resolution Universe South Low Latitude (HTRU-S LowLat) pulsar survey by implementing a pulsar search pipeline that was previously used to reprocess the Parkes Multibeam Pulsar Survey (PMPS). We coherently searched the full 72-min observations of the survey with an acceleration search range up to $|50|\,\mathrm{m\,s^{-2}}$, which is most sensitive to binary pulsars experiencing nearly constant acceleration during 72 min of their orbital period. Here we report the discovery of 71 pulsars, including six millisecond pulsars, of which five are in binary systems, and seven pulsars with very high dispersion measures (DM $> 800\,\mathrm{pc\,cm^{-3}}$). These pulsar discoveries largely arose by folding candidates to a much lower spectral signal-to-noise ratio than in previous surveys and by exploiting the coherence of folding over the incoherent summing of the Fourier components to discover new pulsars as well as candidate classification techniques. We show that these pulsars could be fainter and on average more distant as compared with both the previously reported 100 HTRU-S LowLat pulsars and the background pulsar population in the survey region. We have assessed the effectiveness of our search method and the overall pulsar yield of the survey. We show that through this reprocessing we have achieved the expected survey goals, including the predicted number of pulsars in the survey region, and discuss the major causes why these pulsars were missed in previous processing of the survey.

Key words: surveys – stars: neutron – pulsars: general.

1 INTRODUCTION

The quest for new radio pulsars stands as a major and ongoing objective in the field of pulsar astronomy. Since their discovery in 1967 (Hewish et al. 1968), the tally of pulsars has climbed steadily and has now reached 3748[1] according to version 2.5.1 of ATNF pulsar catalogue (Manchester et al. 2005). Pulsars have emerged as celestial beacons of immense scientific value as they have dramatically advanced our understanding in many areas of physics and astrophysics (Stairs 2004), such as in testing General Relativity and other alternative theories of gravity in the strong field regime using binary systems (e.g. Kramer et al. 2021), providing evidence of a gravitational wave background (e.g. Agazie et al. 2023; Reardon et al. 2023), constraining the equation of state using pulsar masses (e.g. Cromartie et al. 2020), testing theories of binary stellar evolution, and interactions in close binary systems (Tauris

★ E-mail: rahul.sengar@aei.mpg.de
[1]https://www.atnf.csiro.au/research/pulsar/psrcat/

et al. 2017). Although millisecond pulsars (MSPs) play a crucial role in achieving the aforementioned goals, the majority of known pulsars, around 82 per cent, are normal pulsars with spin periods greater than about 30 ms. These pulsars also provide insights into the enigmatic origin of pulsar emission, which has been a topic of debate among researchers for decades (e.g. Philippov, Timokhin & Spitkovsky 2020). They also provide a window for mapping the Milky Way's pulsar population as well as extremes of the pulsar population, spanning from young to old, high to low magnetic fields, and slow to fast spins, offering valuable insights into the mechanisms behind radio pulse generation (e.g. Tan et al. 2018). The study of nulling and intermittent pulsars is essential for understanding pulsar emission mechanisms (e.g. Konar & Deka 2019). Beyond their individual properties, the pulsar distribution in the Galaxy is also crucial for understanding their population, beaming fraction, birth rate, and local star-formation and supernova rates (e.g. Frail, Goss & Whiteoak 1994). Analysing pulsar scale heights also refines formation models and velocities (Arzoumanian, Chernoff & Cordes 2002). Normal pulsars, abundant and observable at varying distances, offer crucial data for Milky Way cartography, aiding in providing an understanding of the Galaxy's structure, matter distribution, and stellar dynamics (e.g. Dirson, Pétri & Mitra 2022). Normal pulsar rotation measures (RMs) are vital for studying the large-scale structure of the Galactic magnetic field (Han, Manchester & Qiao 1999). These pulsars also serve as probes for studying pulse scattering and enhancing Galactic electron density modelling (e.g. Cordes & Lazio 2002; Yao, Manchester & Wang 2017; Ocker, Cordes & Chatterjee 2020).

Given the multitude of applications of both MSPs and normal pulsars, searching for them has become one of the key science goals for the future Square Kilometer Array (SKA; Levin et al. 2018). While the new pulsar population continues to grow through large-scale pulsar surveys with state-of-the-art radio telescopes such as the 500-m FAST in China (Han et al. 2021) and the 64-dish MeerKAT radio telescope in South Africa (Padmanabh et al. 2023), the reprocessing of existing archival data sets has also been crucial in increasing the pulsar population. A notable example of this practice is the analysis of the Parkes Multibeam Pulsar Survey (PMPS). Over the past two decades, with improvements in search techniques, candidate sifting, folding, and classification methods, the yield of the PMPS has increased by ~ 50 per cent (Faulkner et al. 2004; Mickaliger et al. 2012; Eatough et al. 2013; Knispel et al. 2013) when compared with the pulsar yield through its initial processing. Furthermore, advances in computing power, especially the utilization of graphical processing units (GPUs) in pulsar searches, have enabled a more thorough exploration of previously untapped search spaces at significantly faster rates (e.g. Morello et al. 2019; Sengar et al. 2023). These reprocessing efforts have not only increased the pulsar population through the discovery of many interesting pulsars, but have also resulted in a new class of pulsar termed rotating radio transients (McLaughlin et al. 2006; Keane et al. 2011). Another remarkable example of the reprocessing of pulsar survey data is the discovery of the first fast radio burst (FRB; Lorimer et al. 2007), which was made through reprocessing archival data from a 1.4-GHz survey of the Magellanic Clouds using the multibeam (MB) receiver of the 64-m Parkes Radio Telescope (Manchester et al. 2006).

In this paper, we present new results from a GPU-accelerated reprocessing of 87.3 per cent of the High Time Resolution Universe South Low Latitude (HTRU-S LowLat) survey, with the main aim being to search for accelerated (i.e. binary) pulsars. In Section 2, we give a brief introduction to the HTRU-S LowLat survey (Keith et al. 2010), touching on previous searches for relativistic binary pulsars and the abundance of computational resources now available that provided the motivation for its reprocessing. Section 3 provides an overview of the data analysis methods applied to reprocess the 72-min integration-length observations of the survey. Candidate confirmation and results, including new pulsar discoveries, are summarized in Section 4. Notable pulsar findings are further detailed in Section 5. The redetections of many of these new pulsars in the PMPS survey are briefly described in Section 6. In Section 7, we present a statistical comparison of the new pulsars against previous HTRU-S LowLat pulsars. Survey and pipeline efficiency are addressed in Section 8. In Section 9, we give some insights into potential reasons why the pulsars reported in this work eluded detection in the previous two processings of the survey. Finally, discussions and conclusions can be found in Section 10.

2 HTRU-S LOWLAT PULSAR SURVEY AND ITS REPROCESSING

Over a decade ago three major pulsar surveys of the southern sky were conducted as part of the HTRU project (Keith et al. 2010), using the 13-beam 20-cm MB receiver (Staveley-Smith et al. 1996) of the 64-m Parkes radio telescope (also knows as 'Murriyang') between 2008 and 2013. The high-latitude ($\delta < +10^\circ$) part of the survey (HiLat) unveiled the cosmological population of FRBs (Champion et al. 2016), the mid-latitude ($|b| < 15^\circ$, $-120^\circ < l < 30^\circ$) part of the survey (MedLat) found a rich pool of MSPs and a bright magnetar (Levin et al. 2010), whilst the low-latitude ($|b| < 3.5^\circ$) part of the survey (HTRU-S LowLat) was tailored to detect relativistic binary pulsars and probe the low-luminosity end of the pulsar population. It is worth noting that while the PMPS had previously observed the same sky region using the MB receiver, the HTRU-S LowLat survey surpassed it in technological prowess. This was achieved through a 10-fold increase in frequency channelization, where the number of frequency channels increased from 96 in the PMPS to 1024 in HTRU-S LowLat, although the total observing bandwidth was not significantly different, namely 288 MHz for PMPS and 340 MHz for HTRU-S LowLat.[2] Additionally, a finer time resolution was adopted, featuring a sampling rate of 64 μs compared with the PMPS's 250 μs. The integration length was also extended, doubling from 36 min in the PMPS to a comprehensive 72 min in HTRU-S LowLat. These sensitivity enhancements made HTRU-S LowLat a technological successor to the PMPS, ensuring that it was more sensitive for detecting MSPs and highly scattered as well as fainter pulsars that potentially were missed or not detected in the PMPS.

The first search for the relativistic binary pulsars in 50 per cent of the data of the HTRU-S LowLat survey was conducted by Ng et al. (2015) with a CPU-based, partially coherent segmented acceleration search pipeline, and it discovered 60 pulsars. This pipeline used a 'time-domain resampling' acceleration search technique, which is sensitive when the length of the observation is 10 per cent of the orbital period of a binary system, namely $t_{\rm int}/P_{\rm orb} \leq 0.1$, where $t_{\rm int}$ is the integration time and $P_{\rm orb}$ is the orbital period of a pulsar in a binary system (Ransom, Cordes & Eikenberry 2003). Therefore, to detect highly accelerated binary pulsars, each 72-min observation of the HTRU-S LowLat survey was divided into full-length, half-length, quarter-length and eighth-length segments, and an acceleration search (up to a maximum acceleration of 1200 m s^{-2})

[2] The total HTRU-S LowLat bandwidth was 400 MHz, with a channel bandwidth of 0.390 MHz. However, 150 channels were consistently affected by RFI, making the effective bandwidth 340 MHz.

was performed separately on 15 segments of each observation. This segmentation provides sensitivity to binary pulsars with successively shorter orbital periods. Without employing this approach, potential highly accelerated pulsars might have remained undetected due to the deleterious effects of Doppler smearing caused by the binary motion in large-integration observations. Later, Cameron et al. (2020) processed 44 per cent of the data using the segmented acceleration search pipeline and discovered 40 pulsars. The first-pass processing of 94 per cent of the HTRU-S LowLat data thus resulted in the discovery of 100 pulsars, with 11 pulsars in binary orbits, including one of the most accelerated binary pulsars, PSR J1757−1854 (Cameron et al. 2018).

While the segmented search approach enhanced the sensitivity for highly accelerated pulsars experiencing noticeable jerk during 72 min of their orbit, there is still room for further refinement in search strategies. Notably, the segmentation search led to a reduction in sensitivity for the full-length observations, scaled by a factor of $\sqrt{n}$, where n represents the number of segments (assuming an equal division). Although the full-length observations were also coherently searched, they were only searched to mild accelerations within the range of $a = \pm 1\,\mathrm{m\,s^{-2}}$. This limitation rendered the detection of faint, accelerated pulsars challenging. Additionally, prior to processing, all original observations in the filterbank format underwent down-sampling by a minimum factor of 2, potentially diminishing sensitivity towards MSPs. Computational limitations at the time of the first search limited the phase space that could be explored.

With the development of GPU-based search codes in recent years, particularly on large-scale GPU clusters, the capacity to swiftly reprocess large amounts of pulsar survey data has become a reality. This technological leap not only has bolstered our ability to process data efficiently, but also has significantly broadened the parameter space available for exploration, resulting in an increase in the likelihood of discovering more pulsars (e.g. Morello et al. 2019; Sengar et al. 2023). Therefore, with the expanded capacity of data processing, apart from the work presented in this paper, two parallel reprocessings of the survey were conducted using different search algorithms. The first involved Keplerian parameter searches for pulsar–black hole binaries in circular orbits by utilizing a template bank algorithm. This technique led to the discovery of 21 new pulsars among which only one pulsar was identified as a MSP in a binary system, with the others being isolated pulsars. The second method employed an acceleration search using the Fast Folding Algorithm (FFA; Staelin 1969), but this analysis was restricted to processing observations only around the Galactic Centre. This processing has resulted in the discovery of a new isolated pulsar, PSR J1746–2829, which has a large dispersion measure (DM) of 1309 pc cm^{-3} and is located just 0°.5 from the Galactic Centre (Wongphechauxsorn et al. 2024). Note that all these pulsars were also redetected later in our reprocessing of the survey.

In this paper we will provide a comprehensive account of our reprocessing efforts by leveraging GPU accelerators on the OzStar supercomputer at Swinburne University of Technology to search for more pulsars in the HTRU-S LowLat survey.

3 METHODS AND DATA ANALYSIS

We developed a pipeline utilizing the GPU-based pulsar search code`PEASOUP,` which was previously used to reprocess the PMPS (see Sengar et al. 2023). Because both the PMPS and HTRU-S LowLat survey used the same MB receiver, only minimal adjustments were required for the pipeline, primarily involving modifications to the parameter search space. The use of `PEASOUP` significantly optimized the most time-consuming tasks in CPU-based pulsar search pipelines, such as the time-domain resampling and Fast Fourier search operations. In this study, `PEASOUP` was deployed on NVIDIA P100 12-GB PCIe GPUs on the OzSTAR supercomputer and achieved an average wall-clock time of 22 ms per trial acceleration for HTRU-S LowLat observations. In comparison, CPU-based codes, such as the `seek` suite within `SIGPROC`, require approximately 19 s for similar operations. This represents an 850-fold increase in processing speed, which is a substantial enhancement in computational efficiency from using GPUs.

3.1 Radio-frequency interference excision

The removal of radio-frequency interference (RFI) was accomplished through a three-step process. First, 155 out of the 1024 frequency channels were identified as contaminated by narrow-band RFI and were always masked during de-dispersion. Subsequently, two multibeam techniques were employed for RFI excision. In the time domain, an ‘eigenvector decomposition’ method (Kocz, Briggs & Reynolds 2010) was used, which involves producing a time series at DM = 0 pc cm^{-3} from each beam and forming a matrix for each time sample by cross-correlating these time series. The matrix was then decomposed into eigenvectors and eigenvalues, with the number of eigenvalues indicating the number of beams in which the signal was present. By applying a threshold, bad time samples contaminated by RFI could be identified and used as a mask in the time domain. In the Fourier domain, a periodic RFI mask was created using the ‘multibeam coincidence technique’, which involves calculating the power spectrum of 13 beams with DM = 0 pc cm^{-3} and applying a cutoff of 4σ to remove any Fourier frequency present in four or more beams. The resulting list of periodic frequencies was called a periodic birdie list (‘birdies’ is a colloquial term for a form of RFI with a relatively pure tone or high Q value).

3.2 Search parameters

As outlined in Section 2, the previous two processings of the HTRU-S LowLat survey faced computational limitations in analysing full-length data with native time resolution, especially in dealing with significant accelerations owing to reliance on the CPU-based pipeline. However, the adoption of the GPU-accelerated pulsar search code `PEASOUP`[3] effectively overcame these constraints. This enabled us to explore wider ranges of acceleration using the survey's full-resolution data set.

To perform coherent reprocessing, we employed the same GPU-based pipeline as discussed in Sengar et al. (2023), with the search parameters outlined in Table 1. Given that the Galactic Centre is the densest region of free electrons in the Milky Way, we considered a DM search range extending up to a maximum DM of 2000 pc cm^{-3}, with $\sim$ 2800 trial DMs. This maximum DM is half of the highest line-of-sight predicted DM towards the Galactic Centre according to the NE2001 (Cordes & Lazio 2002) and YMW16 (Yao et al. 2017) electron density models. However, this is consistent with the highest known DM pulsar SGR J1745-2900, which has a DM of 1778 pc cm^{-3}. Therefore, we believe that the majority of the pulsars presently detectable in the HTRU survey should have a DM within our searched DM range.

[3]https://github.com/ewanbarr/peasoup

Table 1. Search parameters used for re-processing the HTRU-S LowLat survey with PEASOUP.

Parameter	Value
DM_{max} (pc cm^{-3})	2000
$N_{DMtrials}$	2778
DM_{tol}	1.1
W_{int} (µs)	64
$\|a_{max}\|$ (m s^{-2})	50
δa (m s^{-2})	0.05
$N_{acctrials}$	1884
$N_{harmonics}$	32
Total beams	16 153
Beams processed	14 103
Processing time (GPU h)	∼ 430 000

Table 2. Number of DM trials used in each DM range in the reprocessing of the HTRU-S LowLat survey.

DM range (pc cm^{-3})	No. of trial DMs
0–50	357
50–100	270
100–200	346
200–500	503
500–800	265
800–1200	229
1200–2000	289

At the onset of the processing, the version of PEASOUP we used loads the observation file (in filterbank format) into RAM and subsequently generates de-dispersed time series for the specified number of DM trials using the dedisp[4] software package (Barsdell et al. 2012). Additionally, these time series are also stored in RAM prior to conducting periodicity and acceleration searches. However, loading all ∼ 2800 time series would necessitate approximately 170 GB of RAM. Given that OzSTAR provided 192 GB of RAM per node at the time, allocating such a large portion for a single job would impede other CPU tasks. Therefore, we processed each observation into subsets of DM ranges, as shown in Table 2.

To search for binary pulsars, PEASOUP uses a time-domain resampling algorithm (Middleditch & Kristian 1984; Johnston et al. 1992). This method achieves its highest sensitivity when the observation duration does not exceed one-tenth of the pulsar's orbital period. Consequently, for the 72-min HTRU-S LowLat observation, the sensitivity to linear acceleration is most pronounced for binary pulsars with orbital periods exceeding 12 h, subject to a maximum constant acceleration of up to $|50|$ m s^{-2}, resulting in 1884 trial accelerations for each trial DM. Assuming circular orbits, this acceleration range is consistent with a line-of-sight acceleration for a pulsar and a 5 $M_{\odot}$ black hole binary system and covers the line-of-sight acceleration observed in the majority of known binary pulsars.

3.3 Candidate selection and folding

The candidate sifting and folding were also conducted using the methodologies explained in Sengar et al. (2023). The utilization of higher-resolution data in modern pulsar surveys has resulted in a sharp increase in the volume of candidates generated during the search process. This increase poses a significant challenge in determining which candidates should be prioritized for folding, as folding tens of thousands of candidates per observation is infeasible. Traditionally, pulsar searches in the spectral domain employ a false alarm threshold that scales with the number of trials conducted during processing. Candidates falling below this threshold in the spectral domain are often considered to be products of random noise coincidences and hence rejected. However, Sengar et al. (2023) demonstrated that adhering to a fixed false alarm threshold could lead to the overlooking of faint narrow-duty-cycle pulsars when sifting through a substantial pool of candidates. This is because narrow periodic signals often exhibit power distributed across various harmonics in the Fourier domain. When these harmonics are incoherently summed to detect a peak in the power spectrum of the fast Fourier transformation (FFT), the resulting spectral signal-to-noise ratio (S/N_{FFT}) is not optimal. In fact, for narrow-duty-cycle pulsars (δ < 3.0 per cent), the folded signal-to-noise ratio S/N_{fold} can be 1.5 to 2.0 times higher than S/N_{FFT} (see section 2.5.2 in Sengar et al. 2023), and for MSPs it remains more or less similar to S/N_{fold}, being only ∼1.2 times higher. Considering this, we followed the candidate sifting technique proposed by Sengar et al. (2023) and opted not to restrict candidate selection based on a fixed threshold. Instead, we employed varied cutoffs determined by parameters such as spin period, S/N_{FFT}, and the number of harmonics (*nh*), thus ensuring a comprehensive assessment of candidates, even those originating from the FFT noise floor.

Using these candidate filtering criteria, the initial pool of candidates was reduced by factor of about 10–12 per beam. Subsequently, a folding pipeline similar to that employed by Sengar et al. (2023) in reprocessing the PMPS was utilized for post-processing. This pipeline leveraged the dspsr[5] tool to fold candidates based on their designated period, DM, and acceleration. We removed the known bad frequency channels from the data and used the clfd[6] RFI cleaning software. The folding properties of the candidates, such as S/N_{fold}, pulse width, optimized spin period, acceleration, and DM, as well as the diagnostic plots were obtained using the psrchive tool pdmp (Hotan, van Straten & Manchester 2004). Given that visually inspecting all folded candidates is a time-intensive and potentially error-prone task, we adopted the candidate discernment criteria outlined in section 3.1 of Sengar et al. (2023). This approach led to a substantial reduction in the candidate pool, enabling efficient one-person visual inspection within a very small fraction of a PhD candidacy.

4 CANDIDATE CONFIRMATION AND NEW DISCOVERIES

We initially identified 98 promising pulsar candidates during the candidate inspection phase. Among these, 78 were designated as 'class A' candidates, meeting criteria such as a visible and consistent signal in both frequency and time domain with folded S/N_{fold} above 8.8 for normal pulsar candidates and 12 for broad MSP candidates. The remaining 20 candidates fell into 'class B', characterized by tentative visibility and S/N_{fold} below 8.8 or having broad pulse profiles with S/N_{fold} less than 12.

The confirmation and follow-up observations were conducted using the Parkes radio telescope. Initially, eight pulsars were confirmed using the MB receiver. However, due to its decommissioning in October 2020, the newly installed ultra-wide-band (UWL) receiver

[4] https://github.com/ajameson/dedisp

[5] https://sourceforge.net/projects/dspsr/

[6] https://github.com/v-morello/clfd

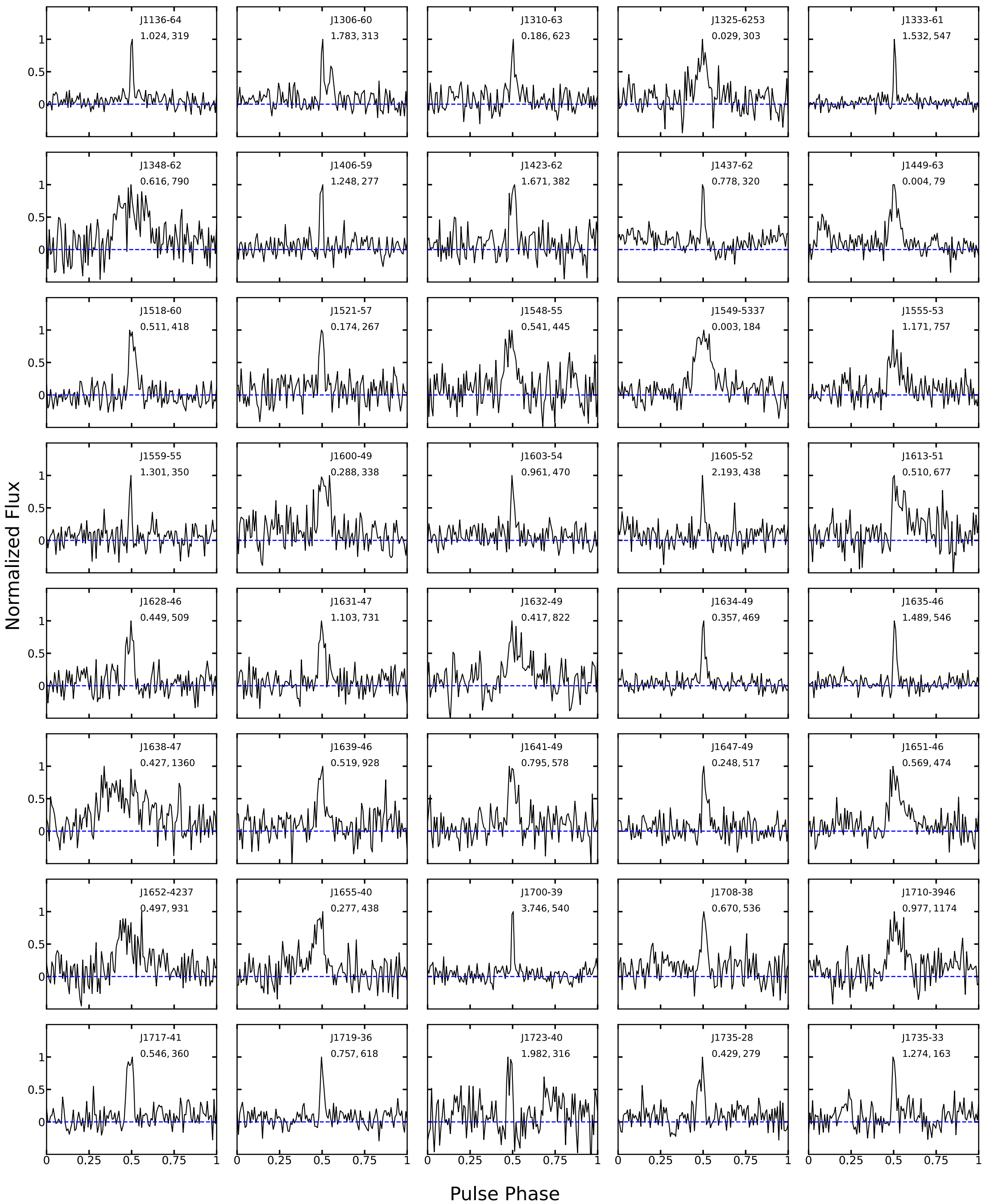

Figure 1. Integrated pulse profiles for the newly discovered pulsars. Each profile contains 128 bins and has been rotated such that it peaks at 0.5 phase. The period in seconds and the DM in pc cm^{-3} are provided for each pulsar.

(Hobbs et al. 2020), spanning 704–4032 MHz, in conjunction with the Medusa backend was used for confirming the remaining pulsar candidates. The confirmation process involved two distinct methods, similar to those utilized in recent reprocessing of the PMPS. The first method, the direct folding approach, employed a UWL frequency subband (1200–1600 MHz) from observations and folded them using the detected period and DM of the candidates. This method successfully confirmed all normal pulsars. However, for MSP and accelerated pulsar candidates, an acceleration search was conducted to determine the optimal folding parameters. Additionally, the analysis of higher-frequency bands provided by the UWL receiver proved instrumental in confirming several faint pulsars that might have otherwise been overlooked due to RFI in the 1200–1600 MHz frequency band, or that would have necessitated additional confirmation attempts.

None of the class B candidates were confirmed as genuine pulsars. In contrast, out of the 78 class A candidates, 71 were confirmed as pulsars, reflecting a 91 per cent confirmation success rate for class A candidates and a 72 per cent overall success rate. This discrepancy in confirmation rates may be attributable to two

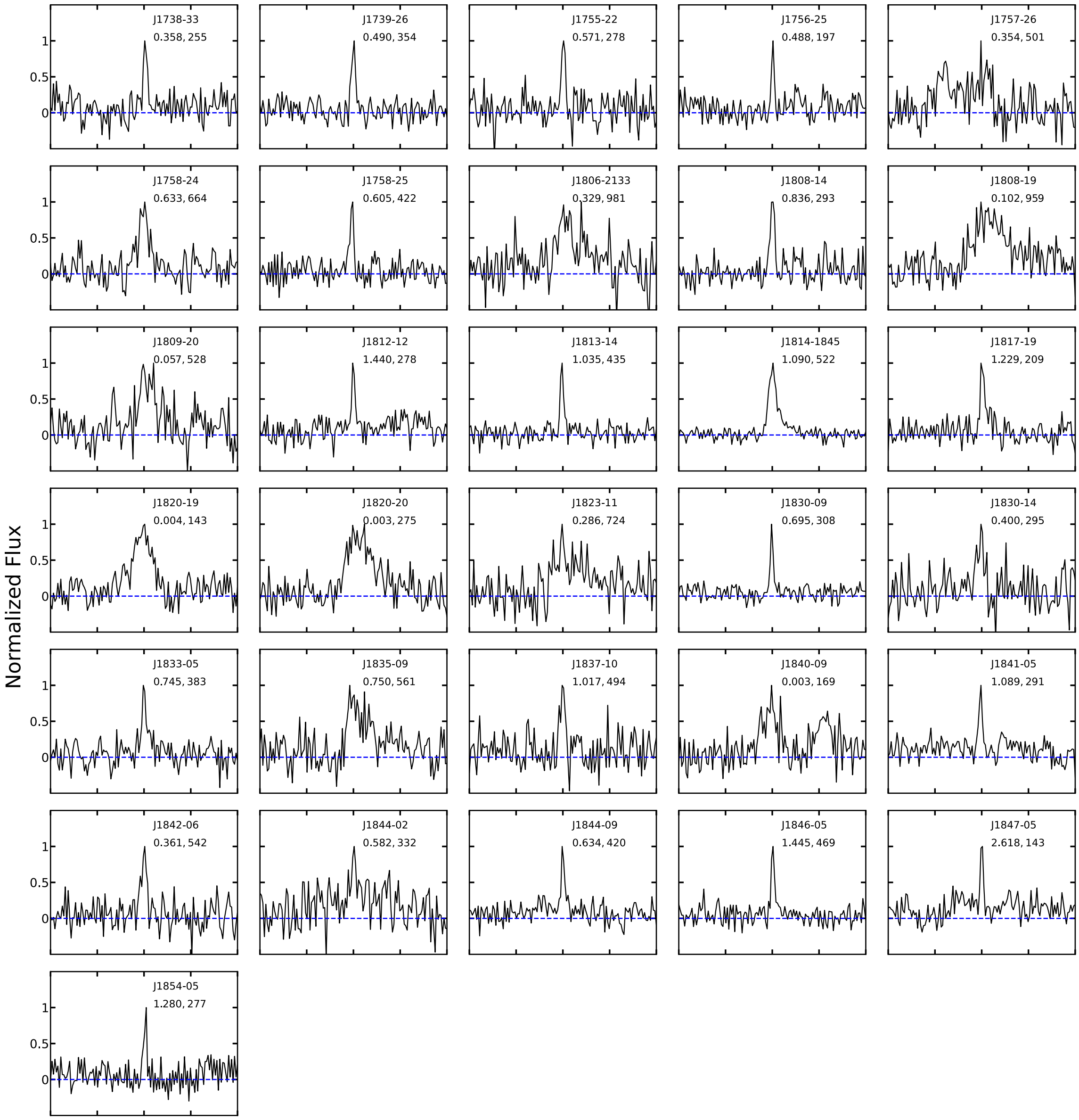

Figure 1. continued.

factors. First, the large number of trial accelerations, coupled with the DM trials, led to false-positive candidates with comparatively higher S/N levels, closely resembling real pulsar characteristics in their candidate plots. Discerning these false positives without direct observation posed a challenge. As for the seven unconfirmed class A slow pulsar candidates, they may potentially belong to the class of intermittent pulsars, necessitating multiple observations for definitive confirmation.

These new pulsars eluded their detection in prior analyses of the HTRU-S LowLat survey, which we attribute to various factors as detailed in Section 9. The basic properties of these newly confirmed pulsars, including spin period, DM, Galactic coordinates from discovery observation, harmonic sums at which they were detected in the FFT power spectrum, S/N_{FFT}, and S/N_{fold} obtained from our pipeline, can be found in Table 3. For each discovery pulse profile of the pulsar, we fitted a Gaussian model using the `lmfit` software package to each profile and reported the pulse width at 50 per cent (W_{50}) of the peak pulse (see Table 4). Furthermore, Fig. 1 showcases a composite view of integrated pulse profiles from the discovery observations.

5 NOTABLE DISCOVERIES

Among the 71 new pulsars reported in this work, PSR J1325–6253 is a double neutron star system and has a remarkably low orbital eccentricity of 0.064, especially given its 1.81-d long orbit (Sengar et al. 2022). Of the other newly identified pulsars, five are MSPs, with four of them being part of binary systems. The remaining pulsars are categorized as normal, with the slowest one having a spin period of 3.7 s. Interestingly, four of these normal pulsars possess relatively fast spin periods (ranging from 50 to 200 ms), suggesting that they may be part of a younger pulsar population. Additionally, one normal pulsar exhibits nulling, and seven pulsars have very high DMs, surpassing 800 pc cm^{-3}. The timing solutions for these pulsars will be addressed in upcoming publications. Therefore, below we

Table 3. Discovery parameters of 71 confirmed new pulsars from ∼87.3 per cent reprocessing of the HTRU-S LowLat survey. The right ascension (RA) and declination (DEC) of these pulsars are the coordinates of the beam centre in which the pulsar was found. The positional error in declination is estimated from the beam size of the MB receiver. The barycentric (BC) spin period (P) in milliseconds and DM values are listed from the discovery observations. The number of harmonics (*nh*) reported here corresponds to the harmonic sums in which the candidate was detected by our pipeline. The parameters S/N_{FFT}, S/N_{HTRU-S} correspond to the S/Ns of the new pulsars obtained in the FFT search and the optimized S/N after folding. S/N_{PMPS} is the folded S/N of pulsar redetection in the PMPS.

PSR name	Pointing/beam	RA (hh:mm:ss)	DEC (dd:mm:ss)	P (s)	DM (pc cm^{-3})	nh	S/N_{FFT}	S/N_{HTRU-S}	S/N_{PMPS}
J1136−64	2012-07-23-00:10:48/10	11:36.4(5)	−64:40(7)	1.0236193(31)	309(10)	32	9.0	14.0	–
J1306−60	2011-12-27-15:02:44/13	13:6.2(5)	−60:21(7)	1.783181(15)	283(28)	32	6.2	11.5	8.2[c]
J1310−63	2012-04-02-09:33:32/10	13:10.3(5)	−63:19(7)	0.18566668(10)	625(2)	16	7.2	9.7	–
J1325−6253[†]	2011-12-10-16:54:46/10	13:25.04.890	−62:53:39.594	0.0289706736(24)	303(0)	8	10.4	14.2	–
J1333−61	2011-09-18-22:03:34/07	13:33.6(5)	−61:48(7)	1.5321347(69)	546(15)	32	12.0	17.3	9.4[c]
J1348−62	2011-10-10-21:55:27/06	13:48.0(5)	−62:30(7)	0.6162574(56)	790(30)	2	7.7	11.0	7.7[c]
J1406−59	2011-04-19-15:27:52/07	14:6.9(5)	−59:23(7)	1.2483120(46)	286(12)	32	9.3	12.8	9.0[c*]
J1423−62	2011-04-23-09:21:43/05	14:23.6(5)	−63:45(7)	1.671473(10)	382(19)	16	5.2	10.0	–
J1437−62	2011-12-05-20:04:47/06	14:37.10(5)	−62:47(7)	0.7779940(17)	323(7)	16	8.6	14.1	10.2[c*]
J1445−63	2012-07-31-11:22:27/12	14:49.8(5)	−63:45(7)	0.003718668530(46)	79(0)	8	13.7	16.0	–
J1518−60	2012-07-31-12:35:11/03	15:18.2(5)	−60:29(7)	0.51065557(77)	420(5)	8	20.2	15.0	–
J1521−57	2013-02-02-16:02:33/12	15:21.8(5)	−57:47(7)	0.173681695(89)	270(2)	8	7.7	10.5	–
J1549−5337[a]	2011-05-18-11:12:03/13	15:49.0(0.5)	−53:37.4(0.7)	0.003316709547(36)	184(0)	4	11.2	13.4	–
J1548−55	2011-12-29-17:55:52/06	15:48.5(5)	−55:54(7)	0.5413823(18)	446(11)	8	5.7	9.0	–
J1555−53	2011-05-17-11:18:22/03	15:55.0(5)	−53:00(7)	1.1708960(88)	785(25)	4	9.1	12.0	10.5[c*]
J1559−55	2012-08-07-03:38:29/05	15:59.9(5)	−55:37(7)	1.3007370(50)	345(13)	32	7.0	10.0	7.9[c]
J1600−49	2012-01-04-18:26:39/04	16:0.4(5)	−49:39(7)	0.28752610(41)	328(5)	8	7.5	10.6	–
J1603−54	2011-12-07-21:23:21/04	16:3.4(5)	−54:05(7)	0.9607924(27)	472(9)	32	8.3	12.6	11.1[c*]
J1605−52	2012-08-03-05:51:26/10	16:5.2(5)	−52:28(7)	2.193373(14)	461(21)	16	5.3	9.2	8.4[c*]
J1614−52[b]	2012-11-26-21:55:56/07	16:14.7(5)	−52:20(7)	0.5099027(18)	673(12)	8	9.2	10.5	10.1[c*]
J1628−46	2011-12-05-03:39:15/04	16:28.0(5)	−46:25(7)	0.44943888(77)	513(5)	8	5.1	9.8	–
J1631−47	2011-12-30-19:34:06/05	16:31.10(5)	−47:10(7)	1.1033263(42)	756(13)	8	7.1	10.4	9.4[c*]
J1632−49	2011-12-13-04:39:04/12	16:32.6(5)	−49:05(7)	0.4168363(16)	814(13)	4	12.3	12.5	–
J1634−49	2011-04-23-20:03:59/02	16:34.6(5)	−49:58(7)	0.35671537(37)	465(3)	16	12.1	15.0	–
J1635−46	2011-06-26-16:09:12/11	16:35.9(5)	−46:45(7)	1.4889028(65)	549(14)	32	10.7	14.9	8.6[c]
J1638−47	2012-04-14-13:41:06/02	16:38.0(5)	−47:50(7)	0.4266682(24)	1374(19)	2	13.2	12.5	12.5[c*]
J1639−46	2012-04-12-12:47:43/13	16:39.2(5)	−46:27(7)	0.5191365(10)	917(7)	4	6.9	9.1	–
J1641−49	2011-10-13-06:08:35/09	16:41.8(5)	−49:34(7)	0.7951897(23)	578(9)	16	5.3	9.9	7.6[c]
J1647−49	2011-10-10-05:13:04/06	16:47.3(5)	−49:10(7)	0.24752785(18)	515(2)	16	8.7	12.6	9.2[c]
J1652−4237[a]	2012-12-30-02:45:46/07	16:52.0(0.5)	−42:37.5(0.7)	0.4965476(21)	943(14)	2	12.7	12.4	15.7[c*]
J1651−46	2011-12-07-22:36:35/04	16:51.1(5)	−46:47(7)	0.5693516(19)	487(11)	4	10.8	13.4	–
J1655−40	2011-04-20-20:48:56/03	16:55.2(5)	−40:10(7)	0.27668901(50)	439(6)	2	9.7	11.9	10.5[c*]
J1700−39	2011-12-10-04:41:41/01	17:0.10(5)	−39:43(7)	3.746463(41)	509(36)	32	10.1	13.5	7.9[c]
J1708−38	2012-03-30-21:22:02/09	17:8.9(5)	−38:04(7)	0.6698359(13)	526(6)	8	6.8	9.3	–
J1710−3946[a]	2011-12-29-20:22:33/01	17:10.8(0.5)	−39:46.3(0.7)	0.9773371(88)	1198(29)	4	6.8	12.8	8.6[c]
J1717−41	2011-10-13-07:22:02/04	17:17.4(5)	−41:19(7)	0.54623299(88)	356(5)	16	12.9	15.4	9.2[c*]
J1719−36	2012-08-03-08:18:01/09	17:19.9(5)	−36:42(7)	0.7571511(16)	624(7)	16	10.1	11.8	7.6[c]
J1723−40	2012-11-25-01:22:55/13	17:23.2(5)	−40:47(7)	1.982265(11)	347(19)	16	11.7	14.0	11.1[c*]
J1735−28	2011-06-27-16:02:05/12	17:35.2(5)	−28:36(7)	0.42856014(65)	279(5)	16	7.4	10.0	–
J1735−33	2012-09-30-05:41:45/11	17:35.10(5)	−33:37(7)	1.2738657(48)	171(12)	32	7.7	10.6	–
J1738−33	2012-10-04-10:29:13/09	17:38.9(5)	−33:52(7)	0.35773440(37)	257(3)	8	6.6	9.7	–
J1739−26	2011-06-30-16:47:36/07	17:39.4(5)	−26:23(7)	0.49014182(78)	354(5)	8	7.2	10.6	–
J1755−22	2011-04-21-19:06:17/08	17:55.3(5)	−22:49(7)	0.57068731(94)	273(5)	32	6.57	8.9	–
J1756−25	2011-04-24-21:02:42/11	17:56.2(5)	−25:18(7)	0.48788974(70)	190(5)	32	6.9	9.4	–
J1757−26	2011-10-06-07:02:33/12	17:57.1(5)	−26:52(7)	0.3544587(26)	502(24)	1	13.9	13.0	9.8[c*]
J1758−24	2011-04-24-21:02:42/03	17:58.3(5)	−24:27(7)	0.6331055(16)	652(9)	4	12.4	13.5	8.3[c]
J1758−25	2013-04-04-17:59:06/13	17:58.9(5)	−25:27(7)	0.6055017(10)	415(6)	32	6.6	9.9	7.6[c]
J1806−2133[a]	2013-01-07-04:18:23/08	18:06.2(0.5)	−21:33.9(0.7)	0.3285584(14)	989(14)	16	8.9	12.9	–
1808−14	2013-04-06-16:18:54/03	18:8.2(5)	−14:57(7)	0.8364221(20)	307(8)	16	7.2	12.0	–
J1808−19	2011-07-02-12:25:09/03	18:8.1(5)	−19:37(7)	0.10166610(10)	969(3)	1	14.2	16.5	–
J1809−20	2013-04-02-16:32:16/06	18:9.8(5)	−20:36(7)	0.057256207(22)	528(1)	2	8.9	11.9	–
J1812−12	2011-12-29-00:45:10/07	18:12.10(5)	−12:54(7)	1.4399673(63)	278(14)	32	5.1	9.7	6.8[c]
J1813−14	2013-04-02-21:22:53/04	18:13.5(5)	−14:44(7)	1.0354074(31)	427(10)	16	9.0	13.4	9.3[c]
J1814−1845[a]	2013-04-08-18:54:20/05	18:14.7(0.5)	−18:45.4(0.7)	1.0899895(35)	534(10)	8	36.1	33.4	8.5[c]
J1817−19	2013-04-08-18:54:20/10	18:17.1(5)	−19:35(7)	1.2290849(44)	191(12)	32	9.0	12.8	–
J1820−19	2012-11-27-01:35:49/04	18:20.6(5)	−19:46(7)	0.004490802565(90)	142(0)	4	15.8	18.8	–
J1820−20	2012-12-10-01:36:29/06	18:20.8(5)	−20:55(7)	0.002699801845(64)	274(0)	4	17.0	18.2	–
J1823−11	2011-12-31-00:27:33/06	18:23.8(5)	−11:48(7)	0.2861844(13)	725(15)	2	9.3	11.0	–
J1830−09	2011-07-05-14:23:13/09	18:30.6(5)	−9:08(7)	0.6954903(14)	309(7)	32	11.2	15.9	–
J1830−14	2011-05-07-15:44:36/13	18:30.1(5)	−14:34(7)	0.39984826(94)	297(8)	8	6.4	9.2	8.8[c]
J1833−05	2012-04-14-19:48:16/08	18:33.2(5)	−05:13(7)	0.7448830(19)	380(8)	16	6.6	11.0	–
J1835−09	2013-04-01-18:01:40/11	18:34.6(5)	−9:15(7)	0.7504618(50)	555(22)	16	10.5	12.5	10.9[c*]
J1837−10	2011-07-14-15:08:44/13	18:37.3(5)	−10:13(7)	1.0166051(36)	493(12)	16	6.0	9.7	–
J1840−09	2013-04-01-19:14:02/07	18:40.6(5)	−09:37(7)	0.003089100596(94)	169(0)	4	10.5	11.6	–
J1841−05	2012-08-03-13:11:46/13	18:41.0(5)	−05:19(7)	1.0885105(35)	274(10)	32	6.0	10.4	–

Table 3 – *continued*

PSR name	Pointing/beam	RA (hh:mm:ss)	DEC (dd:mm:ss)	P (s)	DM (pc cm^{-3})	nh	S/N$_{FFT}$	S/N$_{HTRU-S}$	S/N$_{PMPS}$
J1842−06	2012-08-05-09:30:53/07	18:42.8(5)	−06:21(7)	0.36077664(46)	539(4)	8	7.3	10.4	–
J1844−02	2011-01-03-00:48:46/06	18:44.8(5)	−2:40(7)	0.5815353(12)	336(7)	16	8.5	11.6	8.4[c]
J1844−09	2013-04-01-20:26:44/01	18:44.2(5)	−9:10(7)	0.6344454(11)	415(6)	16	8.5	12.2	10.2[c*]
J1846−05	2012-04-13-20:25:11/06	18:46.2(5)	−5:29(7)	1.4449846(61)	474(14)	32	10.1	14.5	7.5[c]
J1847−05	2011-12-23-03:12:09/01	18:47.7(5)	−05:41(7)	2.618072(20)	170(25)	32	7.4	13.3	–
J1854−05[b*]	2011-12-13-06:05:17/01	18:54.2(5)	−05:12(7)	1.2799447(48)	275(12)	32	9.4	12.4	11.4[c]

Notes.[†] A double neutron star system (Sengar et al. 2022).
[a] Positions were obtained using MeerKAT's FBFUSE and APSUSE backends (Stappers & Kramer 2016). The localization was performed using 480 MeerKAT beams tiled across the area of the MB receiver, and the coordinates of the beam where the pulsar was best detected with the highest S/N are reported.
[b] Later independent discovery in MMGPS-S as PSR J1614−5218, http://www.trapum.org/discoveries/.
[b*] Independent discovery in the Commensal Radio Astronomy FAST Survey (CRAFTS), http://groups.bao.ac.cn/ism/CRAFTS/202203/t20220310_683697.html.
[c] Pulsars found using direct folding.
[c*] Pulsars found in both direct folding and the FFT search.

provide a brief overview of these pulsars. Note that orbital parameters for binary MSPs were determined using `fitorbit`.[7]

5.1 Millisecond pulsars

5.1.1 PSR J1445–63

PSR J1445−63 is a 3.71-ms pulsar with a DM of 79.5 pc cm^{-3}. In our search, it was first identified as a candidate in one of the observations conducted on UTC 2012-07-31-11:22:27, with a mild acceleration indicating the possibility of it being in a binary system. However, several initial attempts to confirm the pulsar were unsuccessful. Subsequently, during the candidate inspection stage, PSR J1445−63 was again detected in two adjacent observations with a mild acceleration, which further indicated that it is a real pulsar in a binary system. A large positional offset between the three observations suggested that the pulsar either was very bright or that its position was recorded inaccurately in the survey metadata. Upon further investigation, erroneous data in the PSRXML header file was discovered, and the corresponding observation was rejected as a probable position of the pulsar. To determine the accurate position of the pulsar, a gridding technique was employed between the two closest observations, and the pulsar was observed for an hour, and we detected it with a high S/N$_{fold}$ of 35.

Subsequent observations of the pulsar revealed that it is indeed a binary pulsar in a 14.09-d orbit with a companion with minimum and median masses of 0.23 M$_\odot$ and 0.27 M$_\odot$, respectively. Additionally, the pulsar exhibits two distinct pulses in its profile, with the interpulse pulse separated from the leading pulse by approximately 194°.

5.1.2 PSR J1840–09

PSR J1840–09 is a 3.089-ms pulsar with a DM of 169.9 pc cm^{-3}. It is present in a binary system and has an orbital period of 5.47 d, with a companion with minimum and median masses of 0.15 M$_\odot$ and 0.17 M$_\odot$, respectively. The pulse profile of this pulsar also shows a strong post-cursor pulse, which is separated by about 110° from its leading pulse.

5.1.3 PSR J1549–5337

PSR J1549−5337 has a spin period of 3.31 ms and the widest orbit of 66 d among the five MSPs reported in this work. Its DM of 184 pc cm^{-3} suggests a distance of 3.9 and 3.5 kpc based on the NE2001 (Cordes & Lazio 2002) and YMW16 (Yao et al. 2017) electron density models, respectively. The minimum companion mass, assuming an orbital inclination angle of $i = 90°$ and pulsar mass of 1.4 M$_\odot$, is 0.20 M$_\odot$, while the median mass, assuming $i = 60°$, is 0.23 M$_\odot$. Despite multiple observations over 219 d, its relatively wide orbit means that phase connection is still incomplete, and high-cadence observations will be required in the future. However, with the precise position measurements obtained using the MeerKAT radio telescope (Stappers & Kramer 2016), we found that PSR J1549−5337 has a narrow pulse profile with a Gaussian full width half-maxima of the pulse, W_{50}, of 0.14±0.01 ms, corresponding to a duty cycle of 4.3 ± 0.2 per cent, whereas the median duty cycle of MSPs with $P < 30$ ms is ~ 9.3 per cent. Continuous monitoring with sensitive telescopes, such as MeerKAT, can provide improved timing accuracy, making this a promising candidate to be included in pulsar timing arrays to detect gravitational waves, unless its high DM makes precision timing difficult.

5.1.4 PSR J1820–20

PSR J1820−20 has a spin period of 2.69 ms, which is the fastest among new MSPs reported in this work. It has a DM of 275.1 pc cm^{-3}, and based on the NE2001 and YMW16 electron density models, it is located at a distance of 5.7 and 10.0 kpc, respectively. This pulsar is in a binary system with an orbital period of 16.3 d, and its companion has minimum and median masses of 0.23 M$_\odot$ and 0.27 M$_\odot$, respectively.

5.1.5 PSR J1820−19

PSR J1820−19 is an isolated MSP with a spin period of 4.49 ms and DM of 143 pc cm^{-3}. Again using the NE2001 and YMW16 electron density models, its distance is 3.1 and 3.2 kpc, respectively. One of the noticeable features of PSR J1820−1946 is that it is detectable across almost the entire UWL band (1000–4000 MHz). The pulsar is highly scattered from 1000 to 1500 MHz, and at higher frequencies the pulse profile is narrower as expected. The formation of isolated MSPs is not well understood and is highly debated; however, there are a variety of formation scenarios. Most plausible scenarios include the formation of massive isolated MSPs via the merging of a neutron star and a massive white dwarf (e.g. van den Heuvel & Bonsema 1984; Bailes et al. 2011) or via the companion's ablation owing to the pulsar wind (e.g. Fruchter et al. 1990).

[7]https://github.com/vivekvenkris/fitorbit

Table 4. Parameters listed in the table are the distances ($D_{\rm NE2001}$, $D_{\rm YMW16}$) of the pulsars using NE2001 and YMW16 electron density models; the minimum flux densities ($S_{\rm min,1400}$) of pulsars assuming the discovery position is the beam centre; W_{50}, the pulse width at 50 per cent of the discovery pulse profiles; and the derived luminosity, $L_{\rm min,1400}$, which corresponds to $S_{\rm min,1400}$ for both the NE2001 and YMW16 models.

PSR name	$D_{\rm NE2001}$, $D_{\rm YMW16}$ (kpc)	$S_{\rm min,1400}$ (mJy)	W_{50} (ms)	L_{1400} (mJy kpc^2)	
J1136−64	7.4,3.4	0.07(1)	18.1±1.8	3.6	0.8
J1306−60	6.7,11.2	0.09(1)	156.1±25.0	4.1	11.4
J1310−63	11.5,12.0	0.06(1)	6.1±1.2	7.8	8.5
J1325−6253	5.4,6.4	0.11(8)	1.7±0.3	3.2	4.5
J1333−61	9.0,12.0	0.07(2)	21.0±1.9	5.8	10.3
J1348−62	13.2,12.8	0.14(1)	144.6±16.0	24.6	23.1
J1406−59	5.2,5.5	0.05(2)	23.8±3.2	1.3	1.4
J1423−62	7.1,6.5	0.05(1)	66.1±10.0	2.4	2.1
J1437−62	6.8,6.4	0.06(2)	16.4±0.0	2.6	2.3
J1449−63	2.2,1.6	0.18(1)	2.2±0.4	0.9	0.5
J1518−60	8.7,15.1	0.10(1)	23.7±2.2	7.7	23.4
J1521−57	4.2,4.5	0.07(2)	5.8±0.9	1.2	1.3
J1549−5337	3.9,3.5	0.24(1)	0.4±6.0	3.6	3.0
J1548−55	6.4,6.5	0.08(1)	42.5±0.026	3.5	3.6
J1555−53	9.6,6.3	0.17(1)	102.6±13.0	15.7	6.8
J1559−55	5.7,6.4	0.04(1)	18.7±2.0	1.3	1.6
J1600−49	9.6,7.1	0.10(1)	23.7±3.2	9.4	5.2
J1603−54	7.2,6.3	0.07(2)	20.2±3.5	3.6	2.7
J1605−52	7.2,4.9	0.07(1)	31.3±2.9	3.5	1.6
J1613−51	10.4,7.6	0.10(1)	114.1±16.0	10.9	5.9
J1628−46	7.3,11.8	0.07(1)	20.0±3.0	4.0	10.2
J1631−47	8.0,6.8	0.10(1)	51.0±6.0	6.9	4.9
J1632−49	9.2,7.1	0.17(1)	67.2±8.0	14.2	8.6
J1634−49	6.6,7.1	0.10(1)	9.7±0.8	4.0	4.7
J1635−46	6.1,5.0	0.12(1)	31.1±2.9	4.5	3.0
J1638−47	17.0,10.0	0.21(1)	141.7±15.0	60.8	20.9
J1639−46	9.3,5.8	0.09(1)	23.6±4.0	7.4	2.9
J1641−49	10.2,18.4	0.10(1)	47.0±6.0	10.7	35.2
J1647−49	9.8,19.0	0.09(1)	9.6±1.3	8.5	32.0
J1652−4237	13.0,25.0	0.20(2)	92.6±6.0	34.9	128.6
J1651−46	6.5,11.1	0.16(1)	60.0±13.0	6.6	19.8
J1655−40	6.7,18.1	0.10(1)	20.6±2.7	4.8	34.9
J1700−39	7.4,16.7	0.06(1)	53.8±7.0	3.3	16.7
J1708−38	6.9,14.2	0.07(1)	21.3±3.1	3.2	13.6
J1755−22	4.3,4.3	0.06(1)	17.8±13.0	1.1	
J1710−3946	12.4,7.1	0.14(1)	108.3±12.0	21.5	7.0
J1717−41	5.6,12.1	0.10(1)	23.2±2.3	3.1	14.7
J1719−36	6.5,4.6	0.11(1)	19.5±2.2	4.8	2.4
J1723−40	4.3,4.2	0.05(1)	60.1±7.1	0.9	0.8
J1735−28	4.4,8.0	0.09(1)	18.0±2.2	1.8	5.7
J1735−33	2.8,3.0	0.07(1)	27.0±3.2	0.5	0.6
J1738−33	3.9,3.9	0.08(1)	8.4±1.6	1.2	1.2
J1739−26	6.0,16.1	0.07(1)	13.1±2.3	2.4	17.0
J1756−25	3.5,3.2	0.06(1)	7.5±1.7	0.7	0.6
J1757−26	7.0,9.3	0.32(2)	125.0±17.0	15.7	27.8
J1758−24	10.6,4.6	0.18(1)	48.7±5.0	20.0	3.8
J1758−25	5.5,4.3	0.09(1)	14.6±1.9	2.8	1.6
J1806−2133	12.2,6.2	0.23(2)	84.4±10.0	34.1	8.7
J1808−14	5.2,8.4	0.06(2)	19.8±2.9	1.6	4.4
J1808−19	11.6,6.3	0.50(3)	24.6±2.2	66.5	19.7
J1809−20	6.6,4.5	0.17(1)	7.4±1.0	7.6	3.5
J1812−12	4.9,5.9	0.050(1)	22.5±2.6	1.2	1.7
J1813−14	6.2,12.2	0.08(1)	20.2±2.3	3.2	12.2
J1814−1845	6.7,4.7	0.42(1)	64.5±3.0	18.8	9.6
J1817−19	3.9,3.8	0.14(1)	38.8±5.0	2.1	2.0
J1820−19	3.2,3.2	0.17(1)	0.60±0.04	1.7	1.8
J1820−20	5.6,9.9	0.17(1)	0.50±0.03	5.4	16.8
J1823−11	8.3,7.0	0.30(2)	82.7±11.0	19.5	13.7
J1830−09	4.6,4.1	0.10(1)	13.4±1.3	2.3	1.8
J1830−14	5.1,5.6	0.07(1)	20.0±4.0	1.8	2.2
J1833−05	6.7,9.3	0.09(1)	31.6±5.0	3.9	7.5
J1835−09	6.7,5.0	0.20(2)	119.5±14.0	9.1	5.0
J1837−10	6.7,11.6	0.07(1)	35.5±4.3	2.9	8.8
J1840−09	3.5,3.7	0.26(2)	1.7±0.32	3.3	3.7
J1841−05	5.3,4.1	0.06(1)	26.8±2.7	1.8	1.1
J1842−06	7.7,6.8	0.06(1)	12.8±2.1	3.8	2.9
J1844−02	5.9,4.5	0.07(1)	24.1±3.5	2.4	1.4
J1844−09	8.2,18.5	0.05(1)	15.1±2.7	3.7	18.8
J1846−05	7.7,9.0	0.09(1)	32.9±4.0	5.2	7.1
J1847−05	3.3,3.7	0.04(1)	39.2±2.0	0.4	0.5
J1854−05	6.0,8.4	0.04(1)	22.6±5.0	1.4	2.8

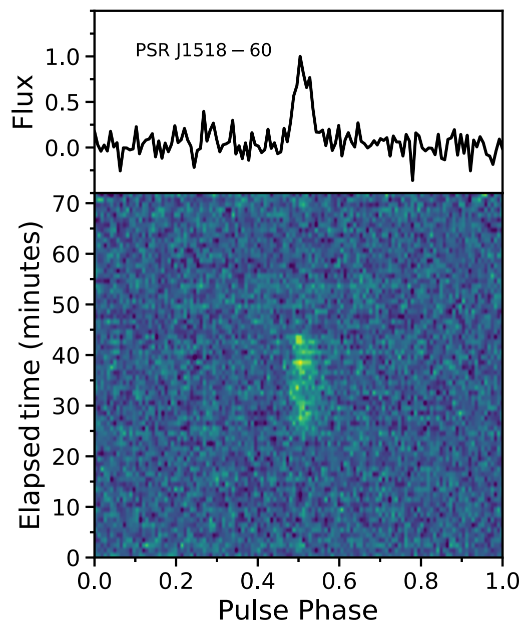

Figure 2. The top panel shows the integrated profile of the nulling pulsar PSR J1518–60, and the bottom plot shows the time-phase plot where the pulsar is visible for only ∼ 25 min.

5.2 PSR J1518–60: A nulling pulsar

PSR J1518−60 exhibits evidence of nulling in its discovery observation and was detected with the high S/N of 15. It shows broadband emission across the entire 350-MHz band and visibility in only ∼ 25 per cent of the observation (see Fig. 2). Apart from this, its relatively high DM of 419 pc cm^{-3} is constrained well away from 0 pc cm^{-3}, with a DM error of only 5 pc cm^{-3}, bolstering the case that J1518−60 is indeed a real pulsar. There have been no further detections of it in 2.9 h of observations taken between MJDs 59216 and 59246 since its initial discovery in the survey, suggesting that it may have a large nulling fraction (NF). Based on the method described in Lyne et al. (2017), the fraction of time during which the pulsar is in the 'ON' state, namely the NF, can be given by $t_{\rm ON}/t_{\rm total}$, where $t_{\rm ON}$ and $t_{\rm total}$ correspond to the time during which the pulsar is visible in the radio or in the 'ON' state and the total observation time, respectively. For J1518−60, the NF in this observation is 73(17) per cent. To further detect this system, observations with a higher cadence or extending over longer durations will be required.

5.3 A collection of high-DM pulsars

Apart from MSPs and a nulling pulsar, there is another class of pulsars, which we term 'high-DM' pulsars. In the new pulsar sample, seven pulsars have DM > 800 pc cm^{-3}, among which PSR J1638−47 and J1710−39 have a DM of 1374(19) and 1198(29) pc cm^{-3}, respectively, and are among the top 10 highest-DM pulsars in the known pulsar population. These two pulsars are present in the PMPS data but due to a low S/N and scattered pulse they remained undetected in previous multiple processings of the survey; however, recently they were reported as an independent discovery by Sengar et al. (2023). The high DM of these pulsars is not surprising, as these pulsars are located along the tangential direction of the Galactic spiral arms. PSR J1638−47 has a DM very close to the maximum DM predicted by the YMW16 electron density model, but it is less than the maximum DM predicted by the NE2001 electron density model. Similarly, the DM of PSR J1651–42 (DM $\sim$ 931pc cm^{-3}) exceeds the maximum DM prediction by YMW16, but it is less than the DM predicted by NE2001. There are five more pulsars whose DM is within the 80 per cent of the maximum line-of-sight DM predicted by either the NE2001 or YMW16 electron density model. The fact that the DM of neither of the pulsars exceeds the maximum DM prediction by both models suggests that they are within the Milky Way.

6 REDETECTION OF NEW PULSARS IN THE PMPS SURVEY

As the entire portion of the Galactic plane surveyed in the HTRU-S LowLat survey overlaps with the region observed in the PMPS, a search for the closest PMPS observations was warranted to determine if any of the 71 new pulsar discoveries reported in this work are also detectable in the PMPS. Two separate searches were conducted for the PMPS observations within one beam-width (14.′4) of the MB receiver from the original discovery position of the HTRU-S LowLat observations. First, we used the 'direct folding method', in which the PMPS observations were folded with the original discovery period and DM of the pulsars, and, on optimizing the periods and DMs of the pulsars, if the pulsar signal is visible above a S/N$_{\rm fold}$ of $\sim$ 7, then it was considered as a redetection. Of the 71 pulsars, 34 normal pulsars were redetected using the direct folding method, among which 28 were detected with S/N$_{\rm fold}\geq$ 8 (Manchester et al. 2001). The remaining six pulsars have a low detection significance, with S/N$_{\rm fold}$ between 7 and 8. Similarly, following the same methodology of direct folding, in the previous analysis of the HTRU-S LowLat survey conducted by Ng et al. (2015) and Cameron et al. (2020), 31 out of 100 pulsars were redetected above this significance level. Therefore, a total of at least 65 pulsars out of 171 are redetected in the PMPS survey using the direct folding method.

In the second approach, a blind FFT search was conducted on the PMPS observations for the 71 new HTRU-S LowLat pulsars. This search spans a DM range from 0 to 1500 pc cm^{-3}. Out of the 34 pulsars detectable through the direct folding method (see Table 3), approximately 45 per cent (15 pulsars) were detected and meet the criterion of having S/N$_{\rm fold}$ greater than or equal to 8.5. However, upon reviewing their candidate plots, 10 pulsars stand out distinctly and are clearly recognizable. Theoretically, these pulsars should have been detected in previous reprocessings of the PMPS survey, but for unknown reasons they remained undetected. It is possible that due to the large number of candidates, they were overlooked during candidate sorting and inspection, or not picked up in standard FFT searches. Additionally, RFI may have contributed to their non-detection. Nevertheless, the detection of $\sim$ 50 per cent (15 out of 34) of these pulsars in FFT searches suggests that RFI likely did not play a significant role in their non-detection.

The majority of these pulsars were identified near the FFT noise floor (with S/N$_{\rm fft}$ < 6) and in higher harmonic sums. For these pulsars, the mean value of S/N$_{\rm fft}$is only 5.9. However, after folding, this value increases to 9.8, representing a roughly 70 per cent boost in the S/N. A similar outcome was observed during the reprocessing of the PMPS presented in Sengar et al. (2023), where these 15 pulsars were detected blindly. However, the original discovery plots of 10 of them clearly resembled a genuine pulsar detection, and therefore they are included as independent discoveries in the PMPS reprocessing (Sengar et al. 2023) (they were originally discovered for the first time in this work). This underscores that our search technique also excels in discovering pulsars that are only detectable near the FFT noise floor and were overlooked in previous processings.

7 STATISTICAL ANALYSIS

7.1 Period, DM, and S/N distribution

A significant increase in new pulsar discoveries by $\sim$ 75 per cent as compared with the previous pulsars found in the HTRU-S LowLAT survey has provided us with a comparable sample of pulsars for evaluating whether our pipeline is identifying pulsars that differ statistically from the previous sample of 100 pulsars reported by Ng et al. (2015) and Cameron et al. (2020) in terms of their spin periods, DMs, and S/Ns. In Fig. 3(a), we present the cumulative distribution of spin periods for both the previous and newly discovered HTRU-S LowLat pulsars. The distributions overlap, indicating no apparent difference in the distribution of pulsar periods. This observation is supported by a two-sample Kolmogorov–Smirnov test (KS test), a robust non-parametric method for comparing two samples, which provides strong evidence in favour of the null hypothesis, signifying that the spin period distributions of the previous HTRU-S LowLat pulsars and the new pulsar sample are statistically indistinguishable.

However, in Fig. 3(b), it is evident that the DM distributions exhibit statistically significant differences, a conclusion corroborated by the KS test with a confidence level of 99.99 per cent and a p-value of $\sim$0.009. The mean and median DMs for the 100 pulsars from Ng et al. (2015) and Cameron et al. (2020) are 355 and 326 pc cm^{-3}, respectively. In contrast, for the new pulsar sample, these values are considerably higher, at 480 and 436 pc cm^{-3}, indicating the sensitivity of the reprocessing towards higher-DM pulsars. Notably, the previous sample of pulsars contains only one pulsar, J1731−3322, with a DM greater than 800 pc cm^{-3} (currently, only 1.9 per cent of known pulsars have DM values exceeding 800 pc cm^{-3}). Conversely, our new pulsar sample includes seven pulsars with DM values surpassing this threshold, further affirming that our search pipeline is probing pulsars with higher DMs.

Fig. 3(c) and (d) illustrate the cumulative distribution of the S/N$_{\rm fft}$ and S/N$_{\rm fold}$ for the two sets of pulsars discovered in the previous and current analyses. The KS test indicates a significant difference in both of these distributions, with both having confidence levels exceeding 99.99 per cent with a p-value of $\sim$1e–07. Specifically, the medians of S/N$_{\rm fft}$ and S/N$_{\rm fold}$ for the 100 pulsars identified in previous analyses are approximately 12.9 and 15.5, respectively. However, for the new pulsar sample, the median S/N$_{\rm fft}$ and S/N$_{\rm fold}$ are 8.9 and 12, respectively, suggesting that our search technique is targeting pulsars near the detection threshold of the survey. This disparity may be attributed to the previous searches predominantly favouring the detection of brighter pulsars, primarily by selecting candidates above a certain S/N threshold. However, further investigation into the survey also reveals other underlying factors contributing to this discrepancy, which we will discuss in Section 9.

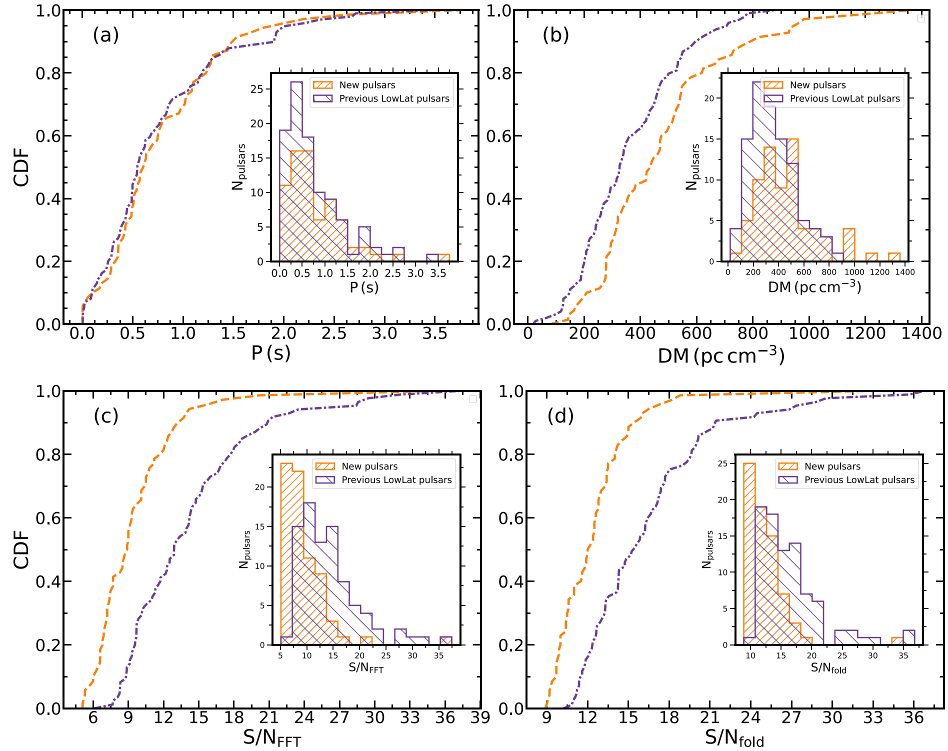

Figure 3. Spin period, DM, S/N_{FFT}, and S/N_{fold} distributions of previously discovered HTRU-S LowLat pulsars (violet) and the new pulsar sample (red) reported in this paper. Each plot shows the cumulative distribution function of each distribution, and inside each plot are histograms of the corresponding distribution.

7.2 Flux density distribution

In an ideal scenario, pulsar flux densities are determined through a two-step process: first by obtaining an optimal position of the pulsar, and then by calibrating the data using the radiometer equation or through comparison with calibration signals that have been referred to other sources of known flux density. However, in cases where calibrated data and the precise pulsar positions are unavailable, we opted to estimate the minimum flux densities at 1400 MHz ($S_{\rm min,1400}$) by assuming the discovery position as the centre of the observing beam. For this estimation, we utilized the pulsar's discovery profile shown in Fig. 1. Our method for flux density calibration is similar to that described in Gitika et al. (2023), which employs the radiometer equation and assumes that the pulsar's off-pulse baseline rms is accurately represented by the sum of the system's equivalent flux density and the Galactic sky temperature, all divided by the antenna gain. The MB receiver has different gain values for its distinct rings: 0.581 $\rm K\,Jy^{-1}$ for the outer rings, 0.690 $\rm K\,Jy^{-1}$ for the inner rings, and 0.735 $\rm K\,Jy^{-1}$ for the centre ring. Therefore, for the flux density estimation, we selected the appropriate gain value corresponding to the beam in which the pulsar was identified. The background sky temperature at the location of the pulsar was obtained from the all-sky catalogue at 408 MHz (Haslam et al. 1982) and scaled at 1400 GHz as $\nu^{-2.6}$. We have provided the $S_{\rm min,1400}$ values in Table 4.

As detailed in Section 7.1, the S/N distribution of the new sample differs significantly from that of the previous 100 HTRU-S LowLat pulsars. Therefore, it is interesting to investigate whether the flux density of the new sample is drawn from a distinct population compared with the previous HTRU-S LowLat pulsars. To compare $S_{\rm min,1400}$ of the new pulsar sample against the previous HTRU-S LowLat pulsars, in Fig. 4 we show the cumulative probabilities of the new sample, previous HTRU-S LowLat pulsars, and the background pulsar population. Although the previous HTRU-S LowLat pulsars are noticeably fainter than the background pulsar population (Cameron et al. 2020), a two-sample KS test analysis revealed that the new sample probes even fainter sources with a significance greater than 99.99 per cent (p-value $< 10^{-5}$).

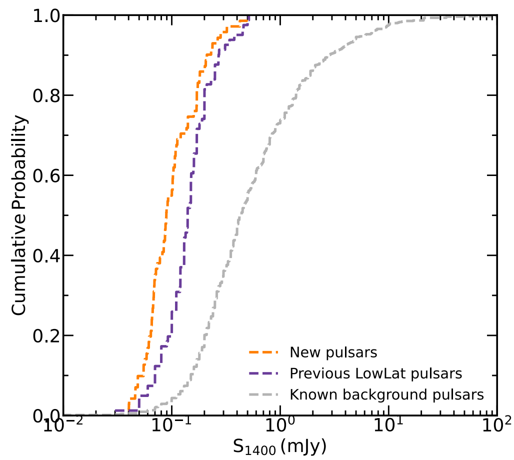

Figure 4. The cumulative distribution function of flux densities of pulsars in the HTRU-S LowLat region. The background pulsars are shown in grey, the previous HTRU-S LowLat pulsars are shown in violet, and the new pulsars reported in this paper are in orange.

However, it is important to note that the true position of the new pulsar sample could potentially alter the flux densities of the new pulsar sample, as the flux density would increase according

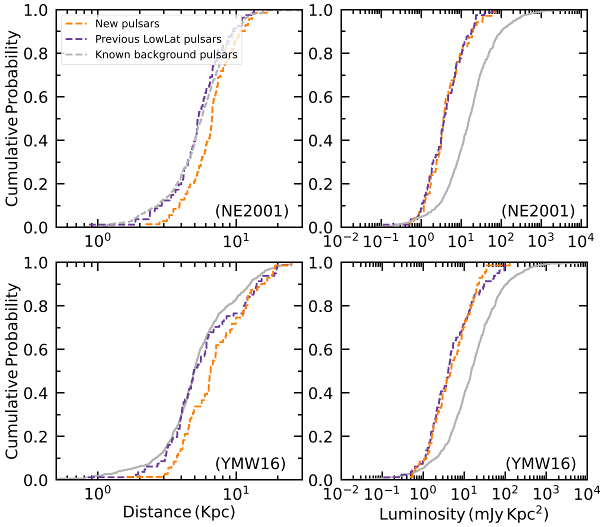

Figure 5. The cumulative distribution functions (CDFs) of the distance and luminosity of the pulsars at 1400 MHz. The known background pulsars are shown in grey, previous HTRU-S LowLat pulsars in violet, and 71 new HTRU-S LowLat pulsars in orange. In the left-hand panels are the CDFs of the distance distribution of each population under both the NE2001 (top) and YMW16 (bottom) electron density models. The corresponding CDFs for the luminosity distribution are shown in the right-hand panels.

to equation (2). To place practical limits on the flux densities of the new pulsar sample, we determined the average positional offset of the previous 88 HTRU-S LowLat pulsars from their discovery observations, relative to the timing positions reported in Ng et al. (2015) and Cameron et al. (2020). This offset was found to be 3.94 arcmin from the beam centre. When comparing the newly obtained flux densities of the new pulsar sample with this offset, the KS test analysis yielded a p-value of 0.014, providing evidence that the new sample is probing relatively fainter pulsars.

7.3 Distance and luminosity

As discussed in Section 7.1, the new sample of HTRU-S LowLat pulsars is probing statistically higher-DM pulsars. This prompted us to investigate whether the DM-derived distances of these pulsars are similar or different. We estimated the distances of all pulsars using the NE2001 (Cordes & Lazio 2002) and YMW16 (Yao et al. 2017) electron density models, and for each model, luminosities were derived using the inverse square relationship, $L = S_{1400} \times D^2$, where D is the model-dependent pulsar distance. The corresponding values of S_{1400} and L_{1400} for each pulsar are listed in Table 4.

In Fig. 5, we show the distance and luminosity comparison of the new 71-pulsar sample, previous HTRU-S LowLat pulsars, and the known background population. When comparing the distance distribution of previous HTRU-S LowLat pulsars against the known background pulsars (shown in the left-hand panel of Fig. 5), the distance distributions of the two populations are similar and consistent with the results obtained by Cameron et al. (2020). However, as confirmed by the KS test with p-values of 0.007 and 0.009, the new pulsar sample is probing more distant pulsars, with a median distance of 6.7 and 6.5 kpc for the NE2001 and YMW16 electron density models, respectively. This distance is 20–35 per cent greater than the previous HTRU-S LowLat and background pulsar population. However, the DM-inferred distances are not well constrained (e.g. Deller et al. 2019); therefore, they should be interpreted with caution.

When comparing luminosities, the KS test indicates that both the previous and the new HTRU-S LowLat pulsars are less luminous than the known background pulsars (p-value $< 10^{-5}$). However, they exhibit similar luminosities when compared with each other. This similarity in luminosity between previous and new HTRU-S LowLat pulsars is likely due to the new pulsars having lower flux densities but larger distances. However, it is important to note that as a result of uncertainties in both the distance and flux density measurements, these luminosity estimates should also be interpreted with caution.

7.4 Scattering

The presence of intervening plasma in the interstellar medium (ISM) leads to the scattering of a pulsar's pulse profiles. This scattering effect is dependent upon the frequency, being more pronounced at lower frequencies and scaling inversely with the fourth power of the frequency; that is, ν^{-4}. Analysing these scattering properties provides crucial insights into the structure of the ISM. It aids in refining models of electron density and mitigating perturbations in times-of-arrival by disentangling scattering effects from the intrinsic pulse profile of the pulsar (Lentati et al. 2017).

Among our recently discovered 71 LowLat pulsars, nine exhibit a visible scattering tail. This characteristic enabled us to conduct a scattering analysis using the software package `SCAMP-I`,[8] which models the pulsar's intrinsic Gaussian pulse profile convolved with an exponential function, $\tau_{\rm scat}^{-1} e^{-1/\tau_{\rm scat}}$, where $\tau_{\rm scat}$ denotes the scattering time-scale. This time-scale scales with frequency as $\tau_{\rm scat} \propto \nu^{-\alpha_{\rm scat}}$.

Due to the low S/Ns of these pulsars, employing subbanded profiles for fitting the model and determining $\tau_{\rm scat}$ at different frequencies and scattering indices was not feasible. Therefore, we integrated the profiles across the entire frequency band and obtained their $\tau_{\rm scat}$. The scattering model fit to the pulse profiles from the original discoveries is shown in Fig. 6. The obtained scattering time-scale values, $\tau_{\rm scat}$, have been normalized to 1-GHz values and are presented in Table 5. Additionally, we show the computed $\tau_{\rm scat}$ using the NE2001 electron density model and scaling relationship from Krishnakumar et al. (2015) at 1.0 GHz, assuming a scattering index, $\alpha_{\rm scat}$, of 4.0.

In Fig. 7, we plot the DM versus $\tau_{\rm sc}$ of these pulsars along with the $\tau_{\rm sc}$ of the known pulsars in the ATNF pulsar catalgue, and clearly the $\tau_{\rm scat}$ of the new pulsars probe the extreme end of the $\tau_{\rm scat}$ distribution. Notably, the values of $\tau_{\rm scat}$ derived from NE2001 and empirical relationships from Krishnakumar et al. (2015) and Bhat et al. (2004) substantially deviate from our measured values for most pulsars. A plausible explanation for these disparities could be the presence of unaccounted foreground structures, such as H II regions in the NE2001 electron density models.

8 SURVEY AND PIPELINE EFFICIENCY

8.1 Redetections of known pulsars

Through an analysis of 14 103 beams in the survey, we identified 792 unique pulsars across 2126 individual beams. These redetections included 86 pulsars among 100 pulsars that were reported as new discoveries by Ng et al. (2015) and Cameron et al. (2020) in their first processing of the survey. The remaining 14 previous HTRU pulsars are present in the beams that have not been reprocessed yet. In addition, we also redetected 87 pulsars (including nine MSPs) in 117

[8] https://github.com/pulsarise/SCAMP-I

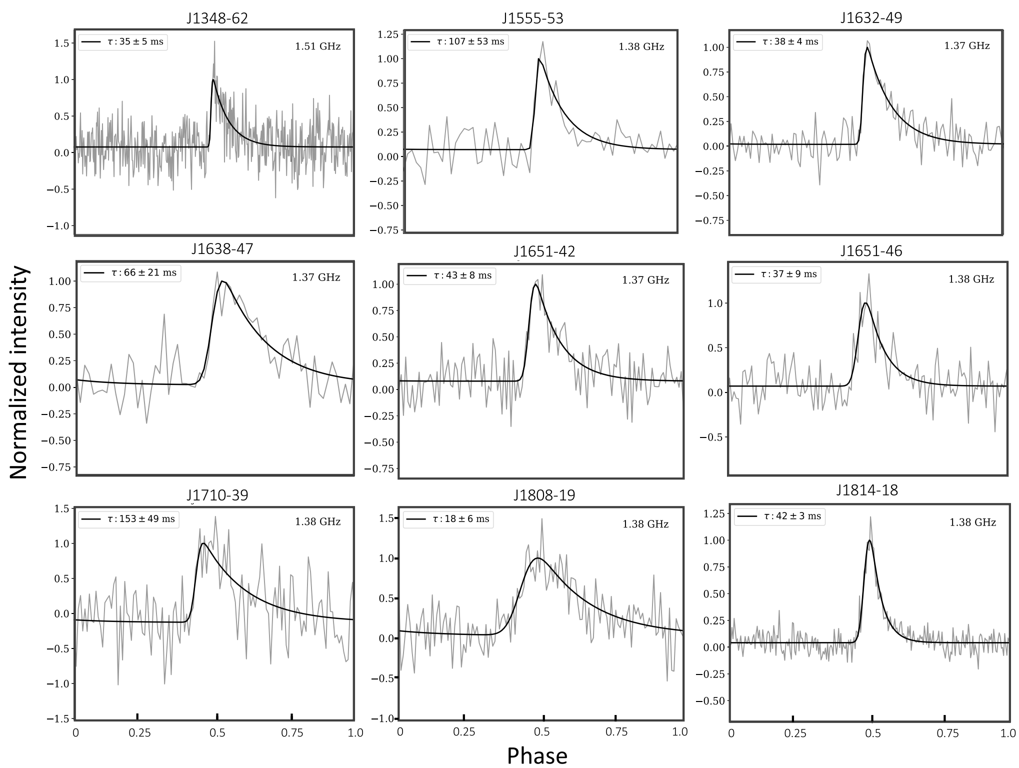

Figure 6. The scatter-broadened pulse profiles (in grey) of newly discovered HTRU-S LowLat pulsars. The solid black line represents the best-fitting pulse-broadening function discussed. In each plot, the value of the scattering time-scale, τ_{sc}, in milliseconds and the effective central frequencies are listed.

Table 5. Pulse scattering parameters obtained by using the model briefly explained in Section 7.4. The values of the scattering time-scale, τ_{scat}, in each case are obtained at the effective central frequency of 1.38 GHz and have been normalized to 1 GHz. Scattering time-scales at 1 GHz predicted by the NE2001 model ($\tau_{scat,\,NE2001}$) and the scaling relationship obtained by Krishnakumar et al. (2015) (τ_{kmn}) assuming a scattering index of $\alpha_{scat} = 4.0$ are given in the last two columns.

PSR name	DM (pc cm^{-3})	τ_{scat} (ms)	$\tau_{scat,\,NE2001}$ (ms)	τ_{kmn} (ms)
J1348−62	790(30)	126(18)	1	18.2
J1555−53	785(25)	388(192)	54	27.3
J1632−49	814(13)	137(14)	54	37.2
J1638−47	1374(19)	239(76)	236	313.1
J1652−4237	943(14)	156(29)	52	66.4
J1651−46	487(11)	134(32)	5	3.5
J1710−3946	1198(29)	562(177)	140	160.0
J1808−19	969(3)	65(21)	97	73.6
J1814−1845	534(10)	152(11)	27	7.0

beams that are present in the survey region but were undetected in the previous processing passes of the survey. To assess the effectiveness of the reprocessing, we conducted a comparison between the detected signal-to-noise ratio ($S/N_{detect} = S/N_{fold}$) and the expected signal-to-noise ratio (S/N_{exp}) for pulsars with an offset, θ, less than half of the full width at half-maximum (FWHM), the value of which is $0\overset{\circ}{.}12$.[9] The expected S/N_{exp} of a pulsar can be computed using the radiometer equation:

$$S/N_{exp} = S_{exp}\frac{G\sqrt{n_p t_{int}\Delta f}}{\beta T_{sys}}\sqrt{\frac{1-\delta}{\delta}}, \quad (1)$$

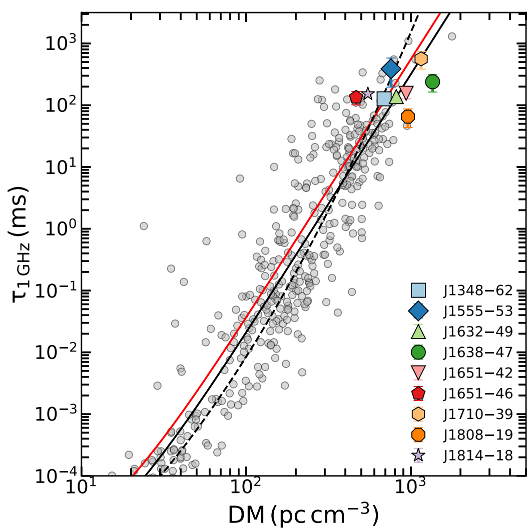

Figure 7. DM versus scattering time-scales of the pulsars presented in this work and reported in ATNF pulsar catalogue with the measurements of τ_{sc} (grey). The dotted black line is the relationship from Bhat et al. (2004), and the solid red and solid black lines represent the relationship between τ and DM obtained by Krishnakumar et al. (2015) scaled at 1 GHz and assuming a scattering spectral index (α_{sc}) of –3.5 and –4.0, respectively.

[9]In this analysis, the offset, defined as θ=FWHM/2 = 0.12, is chosen because the response pattern of the MB receiver deviates from a Gaussian approximation beyond the FWHM of the beam. Observations of known pulsars outside this range can lead to inaccurate S/Ns.

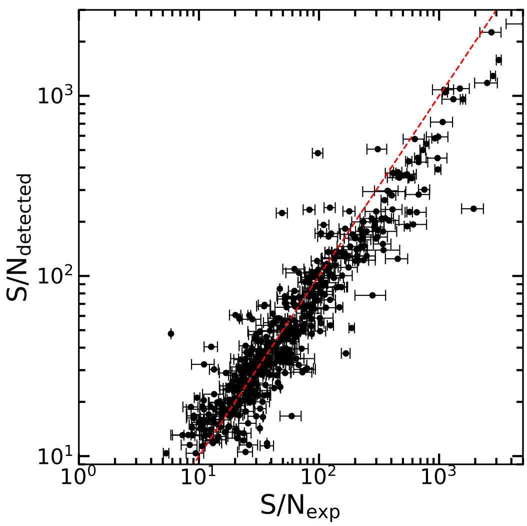

Figure 8. The distribution of observed or detected S/N (S/N$_{\rm detected}$) and expected S/N (S/N$_{\rm exp}$) of 467 unique known pulsars. The red dashed line is the line of quality (1:1 correlation line). The error bars shown are the uncertainties from the ATNF pulsar catalogue .

where $S_{\rm exp}$ represents the expected equivalent continuum flux density (in Jy) of the pulsar, factoring in its degradation due to an offset, θ(in degrees), from its true position. The duty cycle, $\delta = W_{50}/P$, is the fraction of spin period covered by the observed pulse of the pulsar; $n_{\rm p}$ is the number of polarizations; $t_{\rm int}$ is the integration time; and Δf is the effective bandwidth. $S_{\rm exp}$ is calculated using:

$$S_{\rm exp} = S_{1400} \exp\left(\frac{-\theta^2}{2\sigma^2}\right), \quad (2)$$

where σ = FWHM/2.355 is the width of the beam at $e^{-1/2}$ from the beam centre. For a single MB receiver beam, the FWHM is 0°.24, so $\sigma = 0^\circ.1$.

The other terms in the radiometer equation are related to the telescope properties and observational setup. The value of the telescope gain, G (K Jy^{-1}), depends on the telescope size and the beam configuration of the MB receiver, where for the central, six inner, and six outer beams the gain values are 0.735 (K Jy^{-1}), 0.690 (K Jy^{-1}), and 0.581 (K Jy^{-1}), respectively (Keith et al. 2010). The system temperature, $T_{\rm sys}$, is the sum of the receiver temperature ($T_{\rm receiver}$ = 23 K) and the mean sky temperature ($T_{\rm sky}$ = 7.6 K) for the sky region covered by the HTRU-S LowLat survey. The observations are recorded with an integration length of $t_{\rm int}$ = 4320 s, an effective bandwidth of Δf = 340 MHz, and the number of polarizations summed as $n_{\rm p}$ = 2. Finally, $\beta(\geq 1) = 1.16$ is the degradation factor, which accounts for the imperfections that arise due to the digitization of the signal and other effects (Lorimer & Kramer 2004).

The distribution of S/N$_{\rm exp}$ in relation to S/N$_{\rm detect}$ is illustrated in Fig. 8. To ensure the robustness of our analysis, we excluded redetections of pulsars with positional offsets exceeding half of the FWHM of the telescope beam response pattern. This resulted in a selection of 457 unique pulsars for further examination. The majority of detections cluster around the 1:1 line, indicating that the pulsars identified in this reprocessing exhibit the anticipated sensitivity levels. However, the distribution of pulsars around this relationship is not symmetric. Specifically, 279 pulsars (61 per cent) exhibit S/N$_{\rm exp}$ > S/N$_{\rm detect}$. Notably, this trend is more pronounced for pulsars with a high S/N$_{\rm detect}$, exceeding 50. Out of the 262 pulsars with S/N$_{\rm detect}$ > 50, 194 pulsars (approximately 74 per cent) have S/N$_{\rm exp}$ > S/N$_{\rm detect}$. Conversely, for pulsars with S/N$_{\rm detect}$ < 50, the 1:1 relationship is nearly perfect, with only 51 per cent of pulsars exceeding S/N$_{\rm exp}$ > S/N$_{\rm detect}$. These discrepancies may arise from various factors. For instance, the radiometer equation assumes the pulse profile as a top-hat, which is not correct and can result in different values of S/N$_{\rm exp}$; in the case of high-S/N$_{\rm detect}$ pulsars, the sensitivity of the survey may be compromised due to the 2-bit digitization of the HTRU-S LowLat data. Additionally, it is possible that in some cases, the tendency to publish discovery observations, which typically have the highest S/N$_{\rm detect}$ due to scintillation, leads to higher flux densities in the ATNF pulsar catalogue. The influence of scintillation can also result in a relatively large scatter for low-DM pulsars.

Table 6. Expected and actual pulsar detections in the HTRU-S LowLat survey. The table provides an overview of the anticipated and observed pulsar detections from four distinct simulations for the HTRU-S LowLat survey. The values have been adjusted to account for 94 per cent of the survey data. Pulsars are categorized into two groups: 'normal pulsars' (P > 30 ms) and 'MSPs' with (P < 30 ms). The numbers in rows without parentheses or outside parentheses represent the expected numbers of pulsars detectable in 94 per cent of the HTRU-S LowLat survey. Inside parentheses, the first number represents the total number of pulsars detected in the processing, including new discoveries, while the number after the slash ('/') indicates only new pulsar discoveries.

Author	Normal	MSPs
Keith et al. (2010)	900	48
Levin et al. (2013)	–	64
Ng et al. (2015) and Cameron et al. (2020)	960 (723/92)	40 (26/8)
This work	890 ± 27 (879/87)	40 ± 4 (43/7)

8.2 Evaluation of survey yield

Given that we have now reprocessed an equivalent amount of the HTRU-S LowLat data (∼ 87.3 per cent) as compared with the 94 per cent of data previously processed by Ng et al. (2015) (50 per cent) and Cameron et al. (2020) (44 per cent), we are in a position to re-evaluate the survey yield and a comprehensive performance of the survey by comparing with the predictions made using population synthesis-based studies of the survey. In Table 6, we list the pulsar predictions (adjusted for 94 per cent of the survey) made from various population studies. The first population-based study of the survey was conducted by Keith et al. (2010) using PSRPOP[10] (Lorimer 2011) and predicted that the HTRU-S LowLat survey should be able to detect a total of 900 normal pulsars (P > 30 ms). Later, Ng et al. (2015) conducted a similar study using PsrPopPy[11] software (Bates et al. 2014) and found that there should be a total of 960 normal pulsar detections in the survey.

To further refine these predictions, we also conducted simulations using PsrPopPy and found that the HTRU-S LowLat survey should detect approximately 890 normal pulsars and 40 MSPs in 94 per cent of the survey area. However, it is important to note that these numbers carry inherent uncertainties due to the variability in detection methods and the assumptions used in the simulations. Cameron et al. (2020) reported a total of 723 normal pulsar detections from 94 per cent processing of the survey [including 50 per cent of the survey processed by Ng et al. (2015)], which is 20–25 per cent

[10] https://psrpop.sourceforge.net/
[11] https://github.com/samb8s/PsrPOPPy

Table 7. Known millisecond pulsars that were missed in previous analyses of the HTRU-S LowLat survey but redetected in this reprocessing. The exact reasons for their oversight in previous analyses remain unclear; however, it is likely due to human error during candidate inspection or suboptimal data down-sampling. The table lists the pointing/beam in which the pulsar was redetected; the offset (angular distance) from the beam centre to the coordinates in the ATNF pulsar catalogue; P_{cat} and DM_{cat}, namely the period and dispersion measure values from the ATNF pulsar catalogue; S_{exp}, the theoretical S/N of the pulsar calculated from the radiometer equation (assuming a 5 per cent duty cycle); and *nh*, the number of harmonic sums that resulted in a spectral signal-to-noise ratio (S/N_{FFT}). S/N_{fold} is the S/N after folding.

PSR name	Pointing/beam	Offset (°)	P_{cat} (ms)	DM_{cat} ($pc\,cm^{-3}$)	nh	SN_{FFT}	S/N_{fold}	Comments
J1125−6014	2011-12-09-18:06:17/10	0.0978	2.63038	52.951	3	30.4	35.1	Binary pulsar Lorimer et al. (2006)
J1337−6423	2012-04-13-10:37:54/02	0.096	9.42341	259.9	3	20.9	21.5	Intermediate binary pulsar Keane et al. (2011)
J1431−6328	2011-04-17-09:02:20/13	2.080	2.7723	228.2	0	22.9	20.5	Highly polarized source Kaplan et al. (2019)
J1543−5440†	2011-10-09-08:55:32/12	0.11	4.313	102.1	2	11.0	13.0	Binary pulsar Padmanabh et al. (2023)
J1546−5925	2011-04-24-10:48:37/13	0.28	7.8	168.3	3	9.2	11.4	Mickaliger et al. (2012)
J1552−4937	2012-01-19-17:59:08/05	0.10	6.28431	114.6	2	19.7	18.8	Faulkner et al. (2004)
J1652−4838	2012-12-13-20:55:26/03	0.45	3.78512	187.8	1	59.7	52.3	Binary MSP Knispel et al. (2013)
J1725−3853	2011-10-10-06:26:42/07	0.13	4.79182	158.2	1	12.6	13.4	Isolated MSP Mickaliger et al. (2012)
J1748−2446C	2013-04-01-15:35:14/03	0.44	8.4361	237.0	0	15.9	15.8	Lyne et al. (2000)

Note.† We detected PSR J1543–5440 in 2020, but presumed it as a known pulsar found in the HiLat survey. However, upon further review, we recently discovered that it was only listed as a candidate in the HiLat survey and had not been subjected to confirmation observation. The pulsar has now been confirmed and published by the MPIfR-MeerKAT Galactic plane survey as PSR J1543−5439.

fewer detections than predictions for the 94 per cent of the survey. To maintain consistency with the previous processing of the survey, in 87.3 per cent of the survey ∼890 normal pulsars should be detected. As outlined in Section 8.1, aside from the 86 redetections of previous HTRU-S LowLat pulsars, among which 78 are normal pulsars, there have been 706 redetections of known background pulsars, with 670 falling under the category of known normal pulsars. Apart from this, 23 new pulsars were also found in two parallel reprocessings of the survey (see Section 2) using different search algorithms, including one MSP. Therefore, the total new discoveries in HTRU-S LowLat survey are 94, among which 87 are normal pulsars and 7 are MSPs. This brings the overall normal pulsar detection count to 835.

In the remaining 7 per cent of the data there are 14 previously detected LowLat pulsars and 23 known normal pulsars, all of which were redetected by both Ng et al. (2015) and Cameron et al. (2020). If this 7 per cent segment of the survey undergoes reprocessing, we can anticipate the redetection of 37 normal pulsars. Moreover, extrapolating from this, we project the discovery of an additional 7 new normal pulsars. This combined total of 44 pulsars would bring the tally of normal pulsars from 94 per cent of the survey to 879, aligning closely with predictions from simulations, and only slightly below the predictions made by Ng et al. (2015) by a factor of ∼ 8 per cent. Furthermore, it falls short of the predictions by Keith et al. (2010) by only ∼ 2.5 per cent and 1.1 per cent when compared with the population results in this work.

Apart from the normal pulsar population, three different predictions were also made for the MSP population. Keith et al. (2010) and Ng et al. (2015) estimated that HTRU-S LowLat should yield 48 and 40 MSP detections, respectively. In our simulations, we also found that 40 MSPs should be detectable. However, Levin et al. (2013) anticipated a higher MSP yield of 64. Considering the range of estimates (40–64), only 26 MSPs were identified (including 8 new MSPs) in previous processing of the survey, which is 1.5–2.4 times lower than the initial projections. In this work, we have detected a total of 35 previously known MSPs, including 9 MSPs that are present in the survey beams but eluded detection in previous processing (see Table 7). Additionally, 7 more MSPs have also been discovered, resulting in a total count of 42 MSPs in 87.3 per cent of the survey. We also anticipate one additional MSP from the remaining 7 per cent of the data, bringing the total to 43 MSPs. This aligns with the lower limit of predictions, but falls about 20 MSPs short of the upper limit, which may be due to scattering models that are overly optimistic regarding their impact on the MSP population at 1400 MHz.

9 WHY PULSARS WERE MISSED IN PREVIOUS PROCESSINGS

The ∼ 70 per cent increment in survey yield from this latest reprocessing effort raises an intriguing question: Why were these pulsars initially not detected? A comprehensive investigation reveals two major reasons, shedding light on the intricacies of the data processing methods employed previously.

(i) In the initial phases of the processing conducted by Ng et al. (2015) and Cameron et al. (2020), the data underwent a four-fold down-sampling in time prior to FFT and acceleration searches for full-length 72-min observations with $|a| < 1\ \mathrm{m\,s^{-2}}$. For more extreme acceleration searches, the data were further decimated by a factor of 2 in each step. Upon conducting FFT searches for the complete observations of the known pulsars within the survey after down-sampling, we observed an apparent reduction in the FFT signal-to-noise ratio (S/N_{FFT}) of ∼20 per cent for data down-sampled by a factor of 4. This loss increased to about 25 per cent as down-sampling was further intensified. This analysis, performed on hundreds of known pulsars within the survey, yielded consistent results (see Fig. 9). The observed decline in sensitivity arose from suboptimal down-sampling procedures, effectively reducing 2-bit data to 1-bit precision (the scaling factor was incorrect by a factor $4^{1/2} = 2$), leading to an effective 1-bit sampling. It is well known that in the presence

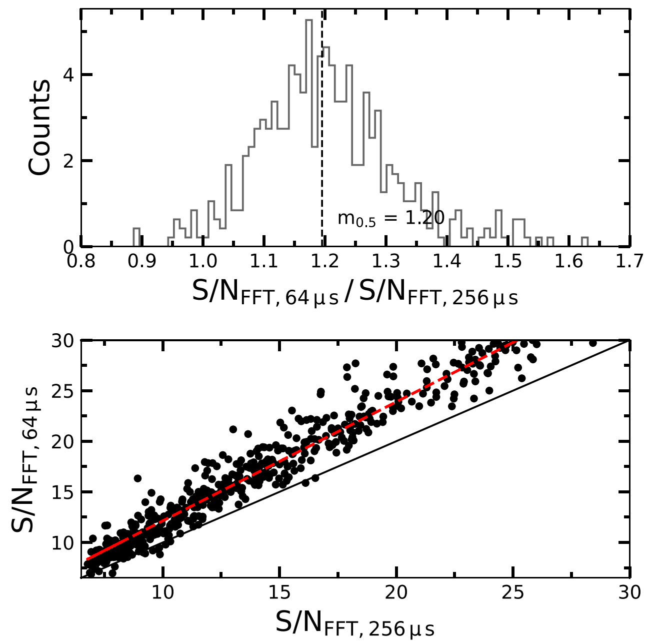

Figure 9. Effect of the incorrect down-sampling algorithm on the FFT S/N. The lower panel shows the distribution of detected FFT S/N for known pulsars by down-sampling the data by a factor of 4 with the incorrect scaling factor ($t_{\rm samp} = 256\,\mu$s) and with full resolution ($t_{\rm samp} = 64\,\mu$s). The dashed red line is the best-fitting line to the distribution, and the solid black line represents the 1:1 ratio. It is clearly visible that for full resolution, the FFT S/N is consistently higher than the down-sampled data. The upper panel shows the histogram of the same distribution, where the median value shows that the full resolution results in an effective increase in the FFT S/N by ~ 20 per cent.

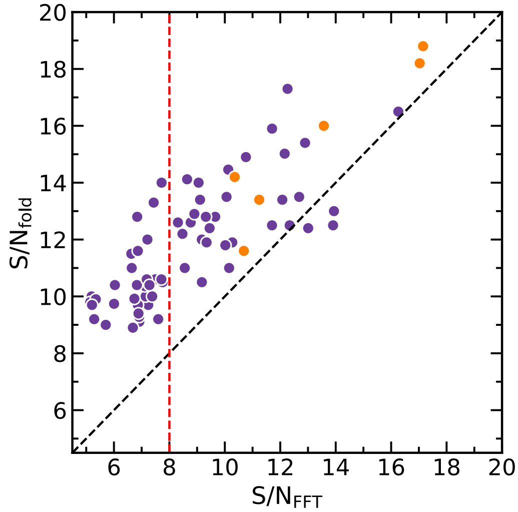

Figure 10. $\mathrm{S/N_{fft}}$ versus $\mathrm{S/N_{fold}}$ of the 71 newly discovered pulsars in the reprocessing of the HTRU-S LowLat survey. The points in violet correspond to the normal pulsars ($P > 30$ ms), while the points in orange are MSPs ($P < 30$ ms). The dashed red line divides $\mathrm{S/N_{fft}}$ pulsars below and above the false alarm threshold of 8, which was used in previous processing passes of the survey. The black dotted line is 1:1, which indicates that the $\mathrm{S/N_{fold}}$ of almost all pulsars is higher than the $\mathrm{S/N_{fft}}$. The high-S/N (33) detection of PSR J1814−18 has been removed to provide clarity for the other data points.

of noise, 1-bit sampling leads to a reduction in the signal-to-noise ratio by a factor of $\sqrt{1/\pi} \approx 0.79$, or approximately 1.25 times. Therefore, the observed losses when down-sampling by a factor of 4 or more align with the characteristics of 1-bit sampling. The extent to which 1-bit sampling affected observations across the entirety of the HTRU-S LowLat survey remains uncertain. However, it is plausible that some pulsars with $\mathrm{S/N_{FFT}} > 8.0$ may have been overlooked during candidate inspection, or that these candidates were simply not considered for further analysis.

(ii) The significant increase in pulsar discoveries can be attributed, in no small part, to the refined candidate selection and folding techniques employed in our study. In the case of the original HTRU-S LowLat survey processing, both MSP and normal pulsar candidates were subjected to a constant false alarm threshold of 8, as assumed by Ng et al. (2015) and Cameron et al. (2020). This threshold was uniformly applied to both $\mathrm{S/N_{FFT}}$ and $\mathrm{S/N_{fold}}$. Additionally, candidates with up to 16 harmonic sums were selected for folding, aligning with the prevailing practice in many previous and ongoing pulsar searches. However, it is a known fact that using a higher number of harmonics, for example 32, can increase the search sensitivity for narrower-duty-cycle pulsars (e.g. Lorimer & Kramer 2004). The analysis of simulated pulsars in Sengar et al. (2023) has also provided a critical insight into this. Due to the effects of incoherent harmonic summing, particularly for narrow-duty-cycle pulsars, the $\mathrm{S/N_{fft}}$ can often fall below the false alarm threshold of 8. Upon folding, the $\mathrm{S/N_{fold}}$ can increase to levels up to 2.5 times higher. This underscores the importance of avoiding high false alarm $\mathrm{S/N_{fft}}$ thresholds in any survey. In retrospect, assuming that accurate down-sampling was executed in prior survey processing phases, it is noteworthy that among the 71 pulsars, 30 exhibited $\mathrm{S/N_{FFT}} < 8$ (see Fig. 10). Intriguingly, out of these, 10 were detected with 32 harmonic sums, suggesting that the inclusion of higher harmonic sums played another helpful role in discovering ~10 per cent of the pulsars that might have otherwise been overlooked with at most a 16-harmonic sum processing.

(iii) While less probable, there are additional factors that could account for missed pulsar detections. Notably, the previous segmented acceleration search pipeline generated an abundance of candidates – approximately 15 times more – leading to an elevated false alarm threshold above S/N = 8 . Consequently, delving deeper into S/N levels revealed previously undiscovered pulsars, resulting in the detection of many pulsars well below $\mathrm{S/N_{FFT}} = 8$. Furthermore, the presence of a known, particularly bright pulsar within an observation can obscure the detection of other, fainter pulsar signals. This occurs because the dominant signal from the bright pulsar overwhelms the candidate list with multiple harmonics, DMs, and accelerations, potentially relegating the weaker pulsar signal lower down the list.

10 DISCUSSION AND CONCLUSION

We have presented a GPU-accelerated search of ~ 87 per cent of the data of the HTRU-S LowLat pulsar survey, utilizing the full 72-min observations at their native time resolution. This coherent acceleration search has led to the discovery of 71 new pulsars, which have been reported for the first time in this study. Simultaneously, two other parallel reprocessing efforts also resulted in another 23 new pulsars (see Section 2), giving 94 pulsar discoveries in these reprocessing endeavours. In particular, this reprocessing effort has significantly increased the new pulsar yield in the survey by $\sim$ 75 per cent, making it arguably one of the most fruitful reprocessings to date in terms of the fraction of new pulsar discoveries as compared with pulsar discoveries in the first reprocessing of any survey (note that the PMPS underwent reprocessing eight times to increase the pulsar yield by ~ 50 per cent). These findings can be attributed to two key factors. First, there was the enhancement in sensitivity achieved by reprocessing the survey data without any decimation and to lesser extent a wider acceleration space. Second, there was the adoption of a technique involving 32 harmonic sums, along with a straightforward yet highly effective candidate sorting from near the FFT noise floor, folding and classification techniques, as detailed in Sengar et al. (2023).

The use of GPUs in this work has significantly improved the processing speed of the survey and achieved a performance nearly three orders of magnitude faster than CPU-based codes (see Section 3). The newer versions of GPUs with increased parallel processing capabilities and higher memory bandwidth would further boost pulsar searching performances. The only bottleneck in our processing was the folding of candidates, as the folding was done with CPU-based codes. Future pulsar searches, such as those conducted with the SKA, are expected to generate a plethora of candidates, making it impractical to fold all of them. In this context, the development and implementation of GPU-based folding software becomes one of the top priorities in pulsar searches.

This reprocessing has effectively met all the primary goals of the survey. It has been successful in finding the predicted number of pulsars for the survey based on population synthesis. However, slight discrepancies remain, particularly in the case of the MSP population, where the survey identified 42 pulsars, including new discoveries, as opposed to the expected 63 (Levin et al. 2013). Furthermore, the reprocessing has excelled in discovering a population of pulsars characterized by a high DM, scattering, and at greater distances, in contrast to the initial sample of 100 pulsars identified in the survey. While these newly found pulsars exhibit lower flux densities, their larger distances place them within the same luminosity distribution as the previously identified HTRU-S LowLat pulsars.

In addition to the discovery of the double neutron star system PSR J1325–6253 (Sengar et al. 2022), this study has unveiled four other millisecond binary pulsars. A comparison of these binary discoveries with the Galactic plane population indicates consistency with the typical ones found in the Galaxy with He-WD companions (refer to Fig. 11). In terms of binary pulsar detections, both Ng et al. (2015) and Cameron et al. (2020) reported a total of 39 binary pulsars (28 known and 11 new). Our reprocessing efforts led to the identification of 48 binary pulsars (32 known, 11 previous HTRU-LowLat, and 5 new). Notably, four known binary pulsars, namely PSRs J1811−2405, J1822−0848, J1837−0822, and J1840−0643, were previously undetected, despite their relatively high S/N_{FFT}. The reasons for their prior non-detections remain uncertain.

Moving forwards, our focus will be on developing precise timing solutions for the pulsars introduced in this study, with the exception of PSR J1325–6253, which has already been published. This endeavour will not only enhance our understanding of the individual characteristics of these pulsars but will also contribute to characterizing the newly discovered population as a whole. While a significant portion of the objectives of the HTRU-LowLat survey have been met in this work, there is still room for improvement. Apart from the discovery of PSR J1325–6253, no relativistic short-orbit binary pulsar has been discovered in this work. One potential explanation for this could be a lack of a jerk search. This was highlighted by the discovery of the highly relativistic binary pulsar PSR J1757–1854 (Cameron et al. 2020), which displayed about a 30 per cent decrease in S/N during full-length observation compared with its half-segment counterpart. As discussed in Section 9, the down-sampling in the original segmented acceleration search fell short of optimal conditions. There could be opportunities to discover faint and highly accelerated binary pulsars by re-implementing the segmented search with the techniques employed in this study.

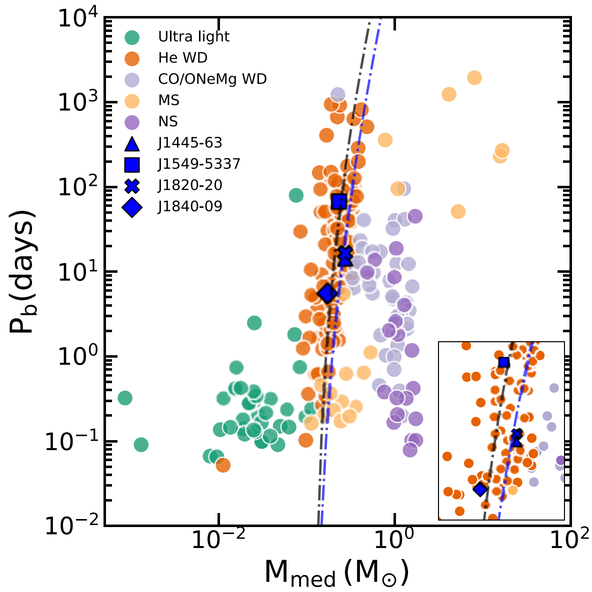

Figure 11. The orbital period (in days) versus median companion masses of Galactic MSPs of different types in binary systems. The data for these systems were taken from the ATNF pulsar catalogue. The new binary MSPs presented in this work are labelled and shown in blue with different markers. The dash–dotted line in blue is the theoretical prediction obtained by Tauris & Savonije (1999) for MSP–He WD systems formed as a final product of low-mass X-ray binaries, and the dash–dotted line in black is the correlation for MSP–He WD systems obtained by Hui et al. (2018).

ACKNOWLEDGEMENTS

The Parkes Observatory is part of the Australia Telescope National Facility (grid.421683.a), which is funded by the Australian Government for operation as a National Facility managed by the Commonwealth Scientific and Industrial Research Organisation (CSIRO). We acknowledge the Wiradjuri people as the traditional owners of the Observatory site. Observations to localize some pulsars used the FBFUSE and APSUSE computing clusters for data acquisition, storage and analysis. These clusters were funded and installed by the Max-Planck-Institut für Radioastronomie (MPIfR) and the Max-Planck-Gesellschaft. The MeerKAT telescope is operated by the South African Radio Astronomy Observatory, which is a facility of the National Research Foundation, an agency of the Department of Science and Innovation. The authors acknowledge support from the Australian Research Council (ARC) Centre of Excellence for Gravitational Wave Discovery (OzGrav), through project number CE170100004 and CE0100016. RS was partially supported by the National Science Foundation (NSF) grant AST-1816904. SS is a recipient of an ARC Discovery Early Career Research Award (DE220100241). RMS acknowledges support through ARC Future Fellowship FT190100155. This research greatly benefited from the OzSTAR supercomputer at the Swinburne University of Technology, a facility supported by both Swinburne University of Technology and the National Collaborative Research Infrastructure Strategy (NCRIS). Without the storage of the archival data and computing resources on OzSTAR, this work would have not been possible. We further acknowledge that these results are based upon work initially presented in Sengar (2023). While the present paper incorporates

moderate modifications, the core of the earlier doctoral work remains intact.

DATA AVAILABILITY

The HTRU-S LowLat data used in this work will be shared on reasonable request to the HTRU-S LowLat collaboration.

REFERENCES

Agazie G. et al., 2023, ApJ, 951, L8
Arzoumanian Z., Chernoff D. F., Cordes J. M., 2002, ApJ, 568, 289
Bailes M. et al., 2011, Science, 333, 1717
Barsdell B. R., Bailes M., Barnes D. G., Fluke C. J., 2012, MNRAS, 422, 379
Bates S. D., Lorimer D. R., Rane A., Swiggum J., 2014, MNRAS, 439, 2893
Bhat N. D. R., Cordes J. M., Camilo F., Nice D. J., Lorimer D. R., 2004, ApJ, 605, 759
Cameron A. D. et al., 2018, MNRAS, 475, L57
Cameron A. D. et al., 2020, MNRAS, 493, 1063
Champion D. J. et al., 2016, MNRAS, 460, L30
Cordes J. M., Lazio T. J. W., 2002, preprint(astro-ph/0207156)
Cromartie H. T. et al., 2020, Nat. Astron., 4, 72
Deller A. T. et al., 2019, ApJ, 875, 100
Dirson L., Pétri J., Mitra D., 2022, A&A, 667, A82
Eatough R. P., Kramer M., Lyne A. G., Keith M. J., 2013, MNRAS, 431, 292
Faulkner A. J. et al., 2004, MNRAS, 355, 147
Frail D. A., Goss W. M., Whiteoak J. B. Z., 1994, ApJ, 437, 781
Fruchter A. S. et al., 1990, ApJ, 351, 642
Gitika P. et al., 2023, MNRAS, 526, 3370
Han J. L., Manchester R. N., Qiao G. J., 1999, MNRAS, 306, 371
Han J. L. et al., 2021, Res. Astron. Astrophys., 21, 107
Haslam C. G. T., Salter C. J., Stoffel H., Wilson W. E., 1982, A&AS, 47, 1
Hewish A., Bell S. J., Pilkington J. D. H., Scott P. F., Collins R. A., 1968, Nature, 217, 709
Hobbs G. et al., 2020, PASA, 37, e012
Hotan A. W., van Straten W., Manchester R. N., 2004, PASA, 21, 302
Hui C. Y., Wu K., Han Q., Kong A. K. H., Tam P. H. T., 2018, ApJ, 864, 30
Johnston S., Lyne A. G., Manchester R. N., Kniffen D. A., D'Amico N., Lim J., Ashworth M., 1992, MNRAS, 255, 401
Kaplan D. L. et al., 2019, ApJ, 884, 96
Keane E. F., Kramer M., Lyne A. G., Stappers B. W., McLaughlin M. A., 2011, MNRAS, 415, 3065
Keith M. J. et al., 2010, MNRAS, 409, 619
Knispel B. et al., 2013, ApJ, 774, 93
Kocz J., Briggs F. H., Reynolds J., 2010, AJ, 140, 2086
Konar S., Deka U., 2019, JA&A, 40, 42
Kramer M. et al., 2021, Phys. Rev. X, 11, 041050
Krishnakumar M. A., Mitra D., Naidu A., Joshi B. C., Manoharan P. K., 2015, ApJ, 804, 23
Lentati L., Kerr M., Dai S., Shannon R. M., Hobbs G., Osłowski S., 2017, MNRAS, 468, 1474
Levin L. et al., 2010, ApJ, 721, L33
Levin L. et al., 2013, MNRAS, 434, 1387
Levin L. et al., 2018, in Weltevrede P., Perera B. B. P., Preston L. L., Sanidas S., eds, proceedings of the 337th Symposium of the International Astronomical Union: Pulsar Astrophysics the Next Fifty Years, Vol. 337, p. 171
Lorimer D., 2011, PSRPOP: Pulsar Population Modelling Programs, Astrophysics Source Code Library. preprint(ascl:1107.019)
Lorimer D. R., Kramer M., 2004, Handbook of Pulsar Astronomy, vol. 4. Cambridge University Press
Lorimer D. R. et al., 2006, MNRAS, 372, 777
Lorimer D. R., Bailes M., McLaughlin M. A., Narkevic D. J., Crawford F., 2007, Science, 318, 777
Lyne A. G., Mankelow S. H., Bell J. F., Manchester R. N., 2000, MNRAS, 316, 491
Lyne A. G. et al., 2017, ApJ, 834, 72
Manchester R. N. et al., 2001, MNRAS, 328, 17
Manchester R. N., Hobbs G. B., Teoh A., Hobbs M., 2005, AJ, 129, 1993
Manchester R. N., Fan G., Lyne A. G., Kaspi V. M., Crawford F., 2006, ApJ, 649, 235
McLaughlin M. A. et al., 2006, Nature, 439, 817
Mickaliger M. B. et al., 2012, ApJ, 759, 127
Middleditch J., Kristian J., 1984, ApJ, 279, 157
Morello V. et al., 2019, MNRAS, 483, 3673
Ng C. et al., 2015, MNRAS, 450, 2922
Ocker S. K., Cordes J. M., Chatterjee S., 2020, ApJ, 897, 124
Padmanabh P. V. et al., 2023, MNRAS, 524, 1291
Philippov A., Timokhin A., Spitkovsky A., 2020, Phys. Rev. Lett., 124, 245101
Ransom S. M., Cordes J. M., Eikenberry S. S., 2003, ApJ, 589, 911
Reardon D. J. et al., 2023, ApJ, 951, L6
Sengar R., 2023, PhD thesis, Swinburne Univ. Technology
Sengar R. et al., 2022, MNRAS, 512, 5782
Sengar R. et al., 2023, MNRAS, 522, 1071
Staelin D. H., 1969, IEEE Proc., 57, 724
Stairs I. H., 2004, Science, 304, 547
Stappers B., Kramer M., 2016, in proceedings of MeerKAT Science: On the Pathway to the SKA — PoS(MeerKAT2016). Sissa Medialab, p. 009
Staveley-Smith L. et al., 1996, PASA, 13, 243
Tan C. M. et al., 2018, ApJ, 866, 54
Tauris T. M., Savonije G. J., 1999, A&A, 350, 928
Tauris T. M. et al., 2017, ApJ, 846, 170
van den Heuvel E. P. J., Bonsema P. T. J., 1984, A&A, 139, L16
Wongphechauxsorn J. et al., 2024, MNRAS, 527, 3208
Yao J. M., Manchester R. N., Wang N., 2017, ApJ, 835, 29

This paper has been typeset from a TEX/LATEX file prepared by the author.